Essentials of Theranostics: A Guide for Physicians and Medical Physicists

Andrew J. H. Sedlack, BS • Catherine Meyer, PhD • Anna Mench, PhD • Celeste Winters, PhD
Dennis Barbon, MD • Sebastian Obrzut, MD • Nadine Mallak, MD

Author affiliations, funding, and conflicts of interest are listed at the end of this article.

Radiopharmaceutical therapies (RPTs) are gaining increased interest with the recent emergence of novel safe and effective theranostic agents, improving outcomes for thousands of patients. The term *theranostics* refers to the use of diagnostic and therapeutic agents that share the same molecular target; a major step toward precision medicine, especially for oncologic applications. The authors dissect the fundamentals of theranostics in nuclear medicine. First, they explain the radioactive decay schemes and the characteristics of emitted electromagnetic radiation used for imaging, as well as particles used for therapeutic purposes, followed by the interaction of the different types of radiation with tissue. These concepts directly apply to clinical RPTs and play a major role in the efficacy and toxicity profile of different radiopharmaceutical agents. Personalized dosimetry is a powerful tool that can help estimate patient-specific absorbed doses, in tumors as well as normal organs. Dosimetry in RPT is an area of active investigation, as most of what we know about the relationship between delivered dose and tissue damage is extrapolated from external-beam radiation therapy; more research is needed to understand this relationship as it pertains to RPTs. Tumor heterogeneity is increasingly recognized as an important prognostic factor. Novel molecular imaging agents, often in combination with fluorine 18–fluorodeoxyglucose, are crucial for assessment of target expression in the tumor and potential hypermetabolic disease that may lack the molecular target expression.

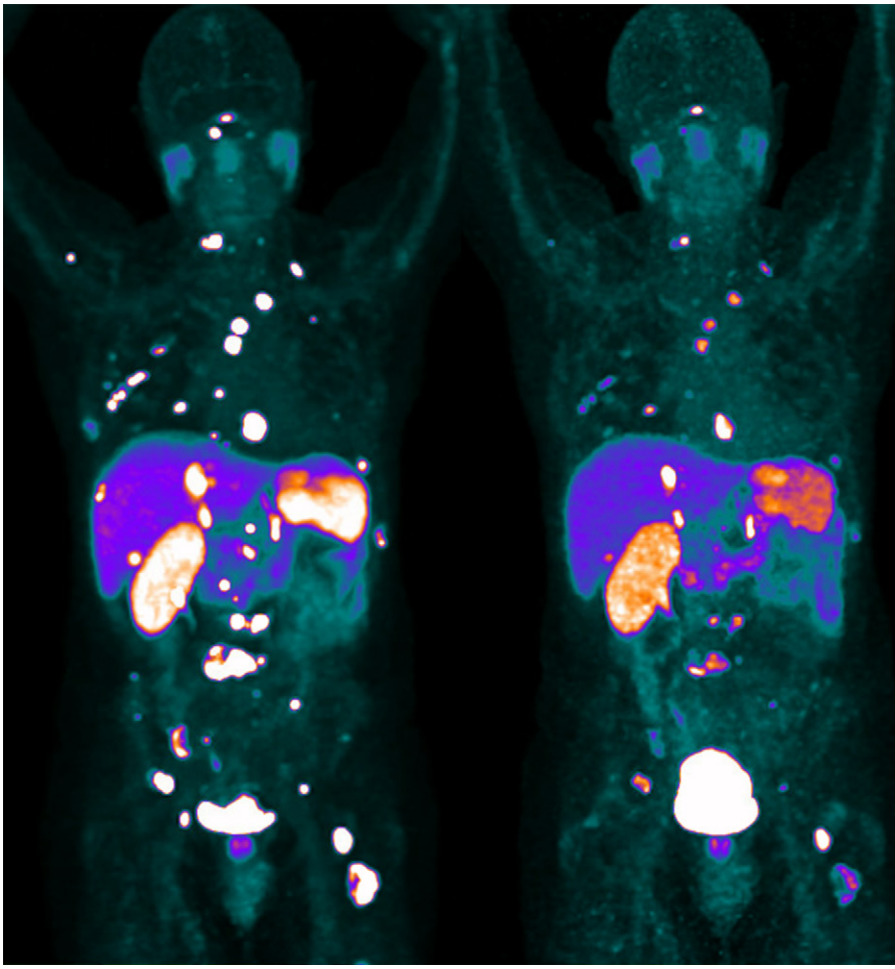

Introduction

The field of radiopharmaceutical therapies (RPTs) dates back to the 1940s, when radioactive iodine emerged for treatment of thyroid pathologic conditions (1). Over the past decade, the field witnessed exciting growth; three therapeutic agents have been approved by the U.S. Food and Drug Administration since 2018 (lutetium 177 [^{177}Lu]–1,4,7,10-tetraazacyclododecane-1,4,7,10-tetraacetic acid [DOTA]-octreotate [DOTATATE], iodine 131 [^{131}I]–metaiodobenzylguanidine [MIBG], and ^{177}Lu–prostate-specific membrane antigen-617 [PSMA-617]), which led to a significant increase in clinical RPT volumes, quickly and increasingly becoming an important aspect of our daily clinical practice (2–4). This expansion is expected to continue, with increased investment in the field and more radiopharmaceutical agents on the horizon.

The term *theranostics* was introduced in the early 2000s as a fusion of the words *therapy* and *diagnostics* to describe the concept of using the same molecular target for imaging and

Supplemental Material

Test Your Knowledge questions are available in the supplemental material.

RadioGraphics 2024; 44(1):e230097
https://doi.org/10.1148/rg.230097

Content Codes: NM, PH

Abbreviations: DOTATATE = 1,4,7,10-tetraazacyclododecane-1,4,7,10-tetraacetic acid–octreotate, FDG = fluorodeoxyglucose, LET = linear energy transfer, MIBG = metaiodobenzylguanidine, MIP = maximum intensity projection, PSMA = prostate-specific membrane antigen, RPT = radiopharmaceutical therapy

TEACHING POINTS

- The damage induced by radiation may be in the form of a single-strand break or double-strand break, depending on the radiation energy, type, and deposition pattern. It is more difficult for the cell to correctly repair double-strand breaks, so radiations that induce more double-strand breaks are more cytotoxic.
- Dosimetry can provide patient-specific estimates of absorbed doses, which can help maximize therapeutic effect while mitigating potential radiation-related toxicity.
- Molecular imaging allows evaluation of the expression of specific molecular targets, their distribution throughout the body, their degree of expression, and the dynamic changes of these features over time.
- The degree of PSMA and DOTATATE uptake at pretherapy imaging serves as a predictive biomarker for response to RPT.
- FDG is a prognostic biomarker; hypermetabolic disease is typically more aggressive and is associated with a worse outcome.

treatment of the same biologic process (5). In this article, we review the core concepts—the whys and hows—of theranostics, or more accurately radiotheranostics, as it pertains to RPTs. Familiarity with the fundamental physics and radiation biology is an imperative starting point to understand the factors that contribute to the therapeutic response and therapy-induced toxicities, as well as the role of personalized dosimetry in individualizing RPTs. Furthermore, tumor heterogeneity plays an important role in predicting tumor response and overall prognosis and deserves an in-depth discussion. A thorough analysis of individual therapies is beyond the scope of this article; instead, we use specific therapies as examples to help explain the core concepts.

Decay Schemes

Given that radiotheranostics—for both imaging and therapeutic applications—hinges on radioactive decay, it is first necessary to understand the different processes of decay. Radioactive decay is the process by which unstable atoms lose energy to become more stable through emission of photons or particles. Types of radioactive decay include γ, electron capture, β-plus, β-minus, and α decays.

Photons (or electromagnetic radiations) are useful for imaging. Radionuclide imaging can be divided into two categories:

1. Gamma imaging—planar or SPECT: Photons produced directly through γ decay or characteristic x-ray emission after electron capture or indirectly using internal bremsstrahlung after β-minus decay, which allows posttherapy imaging.

2. PET: After β-plus decay, the positron emitted—which is an equivalent of a positively charged electron—meets a negatively charged electron in the vicinity, resulting in annihilation interaction and producing a pair of 511-keV photons in opposite directions.

In contrast to electromagnetic radiation, particulate radiation is useful for therapeutic applications and is produced directly through α and β-minus decays or indirectly through Auger electron emission after electron capture (6) (Fig 1).

While neither bremsstrahlung nor Auger electrons are direct forms of nuclear decay, they are often its proximal effects, with bremsstrahlung photons often being emitted after β-minus decay and Auger electrons often being emitted after electron capture (Figs S1, S2).

Decay schemes provide a graphic representation of radioactive decay (Figs 2, 3). Often, radioactive decays are concerted sequences of many individual decays, and certain radionuclides decay via a cascade of events that results in multiple photons, particles, and particle types being emitted (Fig 4).

Radiation Biology

Ionizing radiation has the potential to cause cellular death in normal tissues and tumors by transferring energy and causing strand breaks in the cellular DNA. This can occur in two ways: indirectly by forming unstable free radicals, which inflict damage, or directly, whereby the radiation itself interacts with the DNA. The damage may be in the form of a single-strand break or double-strand break, depending on the radiation energy, type, and deposition pattern. It is more difficult for the cell to correctly repair double-strand breaks, so radiations that induce more double-strand breaks are more cytotoxic. It is well known that the damage capabilities of different forms of radiation are not equal. The important quantities of linear energy transfer (LET) and relative biologic effectiveness (RBE) can help describe the level of radiation damage and over what range it will occur.

LET describes the amount of energy deposition per distance traveled by the radiation. As shown in Table 1, α particles deposit high amounts of energy (LET ~ 80 keV/μm) over a short range (50–100 μm). This makes them useful for highly localized cytotoxic therapy. However, α emitters may also show a recoil effect, whereby daughter radionuclides from the initial decay may have a different distribution than the parents or decay by longer-range (eg, β) mechanisms and therefore irradiate further targets (7). However, β particles deposit less energy per unit path length (LET ~ 0.2 keV/μm) and have a slightly longer range in tissue (up to 12 mm) (Fig 5) (8).

The longest-range radiation with theranostic applications is photons, which deposit little energy per distance traveled and are not appropriate for localized therapy delivery. The average range of photons from γ emitters (eg, ^{99m}Tc) and β^+ emitters (eg, ^{68}Ga, ^{64}Cu, and ^{18}F) is on the order of centimeters in tissues and even more in air, making them well suited for imaging applications. Similar to α particles, Auger electrons have a high LET and a very short range; therefore, they may achieve highly localized DNA damage. Although Auger emitters are not yet often implemented clinically (none approved by the U.S. Food and Drug Administration), animal studies and patient trials using Auger emitters have shown promising results and merit further investigation (8,9).

Diagnostic (electromagnetic radiation)

γ rays	
Charge	0
Relative mass	0 (energy only)
Range in tissue	Long, centimeters in tissue and meters in air
Primary use	Imaging (planar or SPECT)

β^+ particles (positrons)	
Charge	+1 (opposite to e-)
Relative mass	Equivalent to e-
Range in tissue	Long, centimeters in tissue and meters in air (of the 511 KeV photons released by annihilation; range of β^+ before annihilation: millimeters)
Primary use	Imaging (PET) from photons released by annihilation

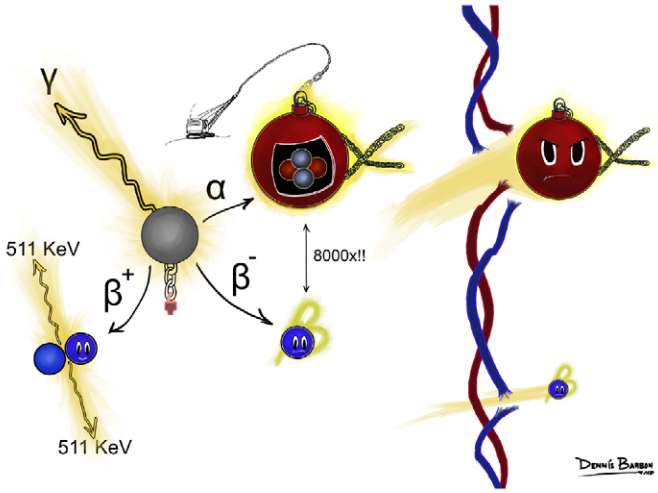

Therapeutic (particles)

α particles	
Charge	+2 (helium nucleus)
Relative Mass	8000 x β
Range in tissue	Short, micrometers
Ionization	Dense, direct action
DNA damage	Double Strand Breaks
Primary use	Highly localized therapeutic

β^- particles	
Charge	-1 (equal to e^-)
Relative Mass	Equivalent to e-
Range in tissue	Medium, millimeters
Ionization	Sparse, indirect action
DNA damage	Single Strand Breaks
Primary use	Relatively localized therapeutic

Figure 1. Types of emitted radiation. Photons (or electromagnetic radiations) are useful for imaging, while particles are useful for therapy. Note how heavy α is, about 8000 times heavier than β. As such, α particles are more effective at cell killing. By definition, γ is emitted from an unstable nucleus, while x-rays are emitted from interactions at the level of the electron shells. Similarly, a particle with a charge of $^-1$ and a mass equivalent to that of an e- emitted from the nucleus is called β minus (β^-), while a similar particle outside (and orbiting) the nucleus is called an electron (e^-).

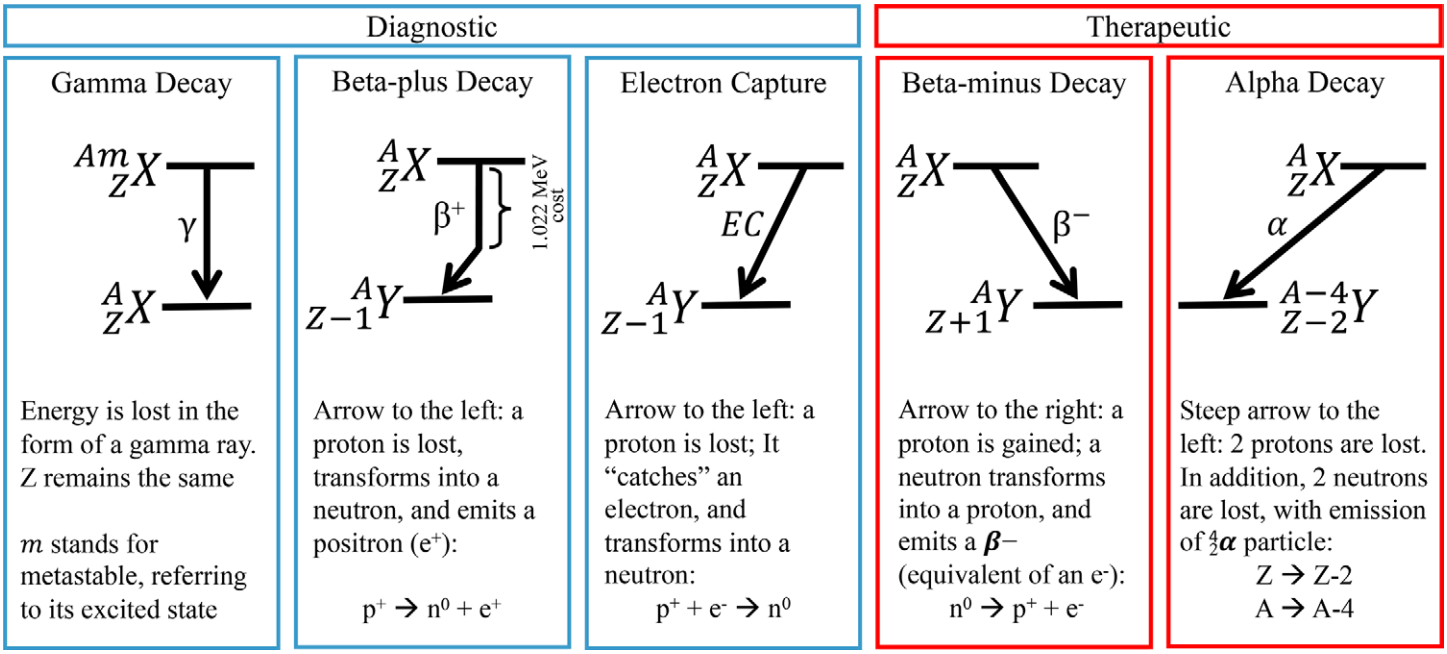

Figure 2. Guide to decay schemes. In decay schemes, the vertical axis represents energy loss, where the height of the vertical drop indicates the amount of energy released, and the horizontal axis represents change in atomic number *(Z)* from parent to daughter radionuclide. Positive change in *Z* is represented by a right diagonal arrow (eg, β-minus [β^-] decay), negative change in *Z* is represented by a left diagonal arrow (eg, α decay), and no change in *Z* is represented by an arrow straight down (eg, γ decay). Note that unlike other decays, β-plus (β^+) decay is drawn as a bent arrow; the initial vertical segment shows the 1.022-MeV energy cost required to emit a β^+ particle, after which the remaining energy (left diagonal arrow) is given to the emitted β^+.

The other important concept that describes a radiation's energy deposition pattern is relative biologic effectiveness (RBE). It is important to distinguish the biologic effect arising from different types of radiation. For example, the same dose from α particles compared with photons will produce different levels of biologic damage. RBE is defined as the ratio of dose needed from a standard defined radiation (usually x-ray) to that of a test radiation to produce equal biologic effect. The

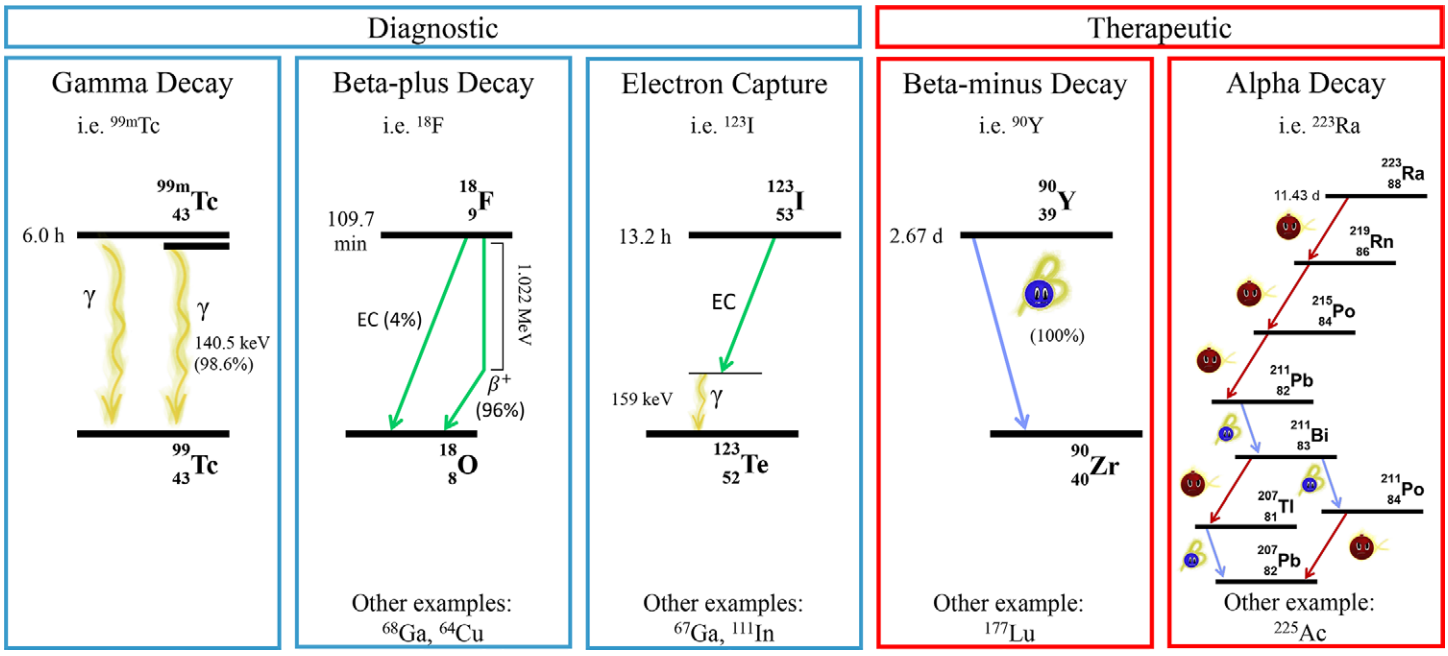

Figure 3. Examples of clinically used radionuclides that decay following each of the decay schemes. *225Ac* = actinium 225, *211Bi* = bismuth 211, *64Cu* = copper 64, *d* = days, *18F* = fluorine 18, *67Ga* = gallium 67, *68Ga* = gallium 68, *h* = hours, *111In* = indium 111, *123I* = iodine 123, *177Lu* = lutetium 177, *min* = minutes, *18O* = oxygen 18, *207Pb* = lead 207, *211Pb* = lead 211, *211Po* = polonium 211, *215Po* = polonium 215, *223Ra* = radium 223, *219Rn* = radon 219, *99mTc* = technetium 99m, *123Te* = tellurium 123, *207Tl* = thallium 207, *90Y* = yttrium 90, *90Zr* = zirconium 90.

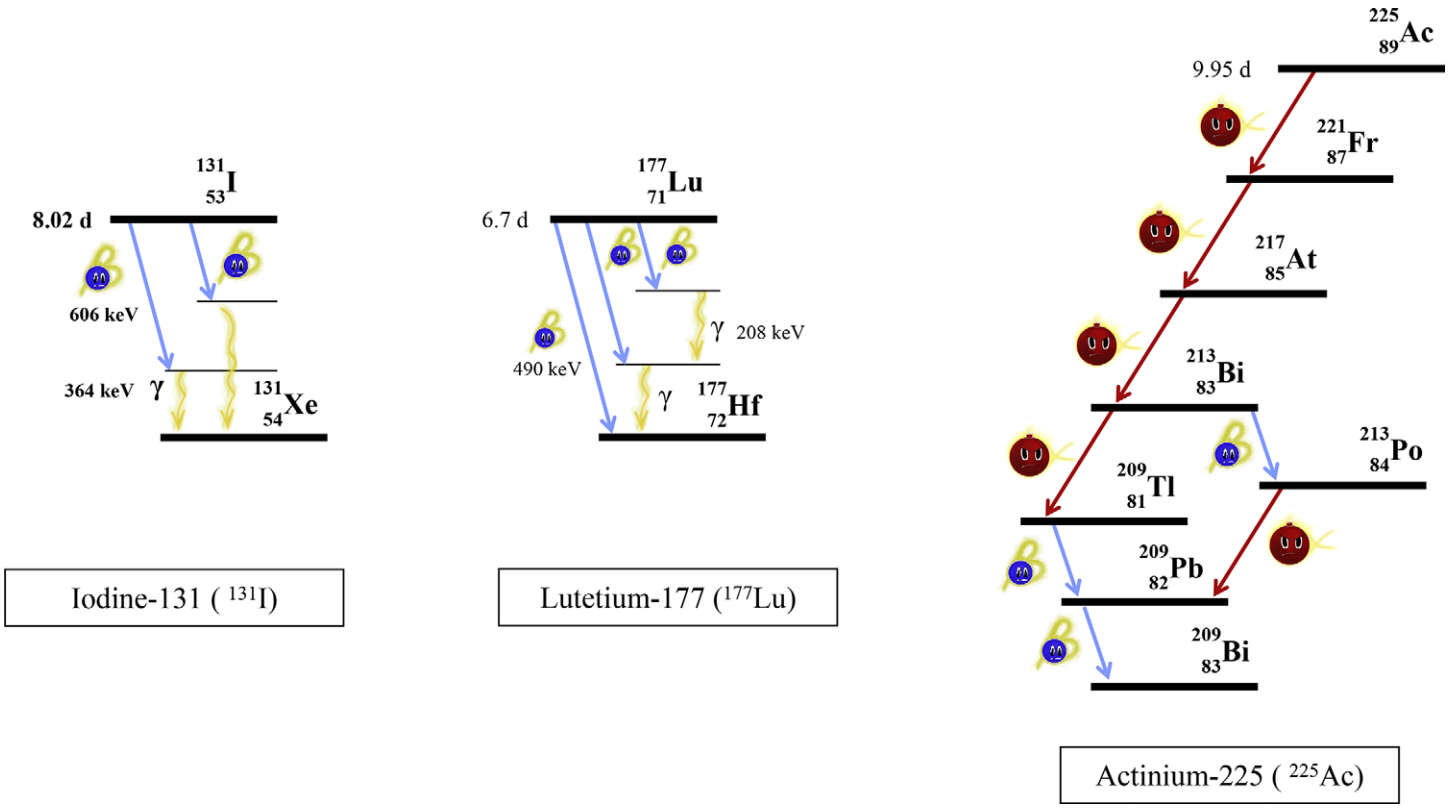

Figure 4. Examples of radionuclides that decay in a cascade of events emitting different photons and particles. Note that in addition to the β-minus emission used for therapeutic purposes, 131I and 177Lu emit photons, which allows posttherapy imaging. 225Ac decays in a cascade of events emitting multiple α particles. *217At* = astatine 217, *209Bi* = bismuth 209, *213Bi* = bismuth 213, *d* = days, *221Fr* = francium 221, *177Hf* = hafnium 177, *209Pb* = lead 209, *213Po* = polonium 213, *209Tl* = thallium 209, *131Xe* = xenon 131.

Table 1: Characteristics and Applications of Emitted Radiation

Type of Emission	LET	Range	Effect	Application
α radiation	+++	+	Dense, highly localized damage	Therapy
β-minus radiation	++	++	Intermediate range and damage	Therapy
γ radiation	+	+++	Sparsely ionizing and long range	Imaging

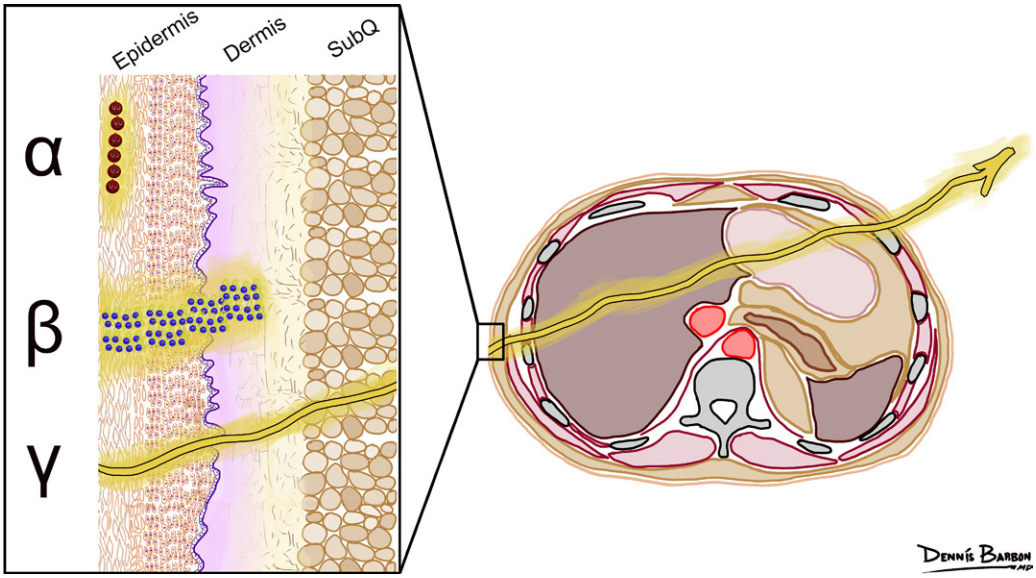

Figure 5. Relative ranges of different types of radiation in tissue. Note that β radiation has a longer range than α radiation in tissue; however, both particles remain relatively localized, causing tissue damage. In contrast, γ radiation has a much longer range; it leaves the body and therefore is useful for imaging. *SubQ* = subcutaneous.

RBE of a radiation type depends on several factors including dose, dose rate, radiosensitivity of cells, repair capabilities, as well as LET. It is also defined for a specific biologic end point, for example, radiation pneumonitis or the proportion of surviving cells in a culture. As with LET, α particles have a high RBE, meaning that they are more efficient at causing damage than β particles or γ emissions (10).

The rate at which a given radiation dose is delivered also affects the biologic outcome. Lower dose rates allow substantially more sublethal DNA damage repair to occur, in contrast to a high-dose-rate delivery. When compared with conventional external-beam radiation therapy (EBRT), which delivers a high level of radiation in a short period (high dose rate), most RPTs are delivered at lower dose rates, diminishing exponentially over time. This has clinical implications for generally accepted toxicity limits for organs at risk like the kidneys, liver, and salivary glands. Currently used dose limits are largely based on data published for EBRT, and more research is needed to determine if higher doses may be tolerated due to the protracted nature of dose delivery with RPTs (11,12).

Radiotheranostic Applications

Typically, theranostic agents consist of a bifunctional compound, with one domain binding to the biologic target and another binding to a radionuclide, often using a chelator (Fig 6). As such, it is possible to label the same targeting agent with an imaging radionuclide to visualize the tumor expression of the target using γ imaging or PET, then subsequently label it with a therapeutic radionuclide for targeted therapy (13,14). The mechanism of action of a prototypical theranostic agent is shown in Figure 7.

Occasionally, the radionuclide itself can serve as the biologic agent, which is the case with our oldest theranostic pair: ^{123}I–sodium iodide (NaI)/^{131}I-NaI, where the iodide is selectively absorbed by thyroid tissue, allowing imaging and treatment of thyroid pathologic conditions (15).

Certain therapeutic radionuclides emit γ or β-plus radiation in addition to the therapeutic particles, which allows posttherapy imaging and imaging-based dosimetry of the therapeutic agent. Clinically, this is most commonly done using the γ emissions of ^{131}I and ^{177}Lu, where posttherapy imaging helps confirm the localization of the therapeutic agent and can help assess treatment response or progression with planar imaging or SPECT/CT performed after serial treatment cycles (Fig 8) (16–18). Common clinical theranostic pairs are summarized in Table 2.

Therapeutic Effect and Toxicity

The therapeutic effect and radiation toxicity of RPTs depend on many factors related to the tumor itself and to patient characteristics, as well as to the therapy administered.

First and foremost, tumor radiosensitivity plays an important role in determining its vulnerability to delivered radiation. Most of what we know on this topic is derived from the EBRT literature. The degree of hypoxia in the tumor microenvironment and the proliferation of cancer stem cells can lead to reduced radiosensitivity and increased genomic instability; hypoxia-inducible factors are associated with the

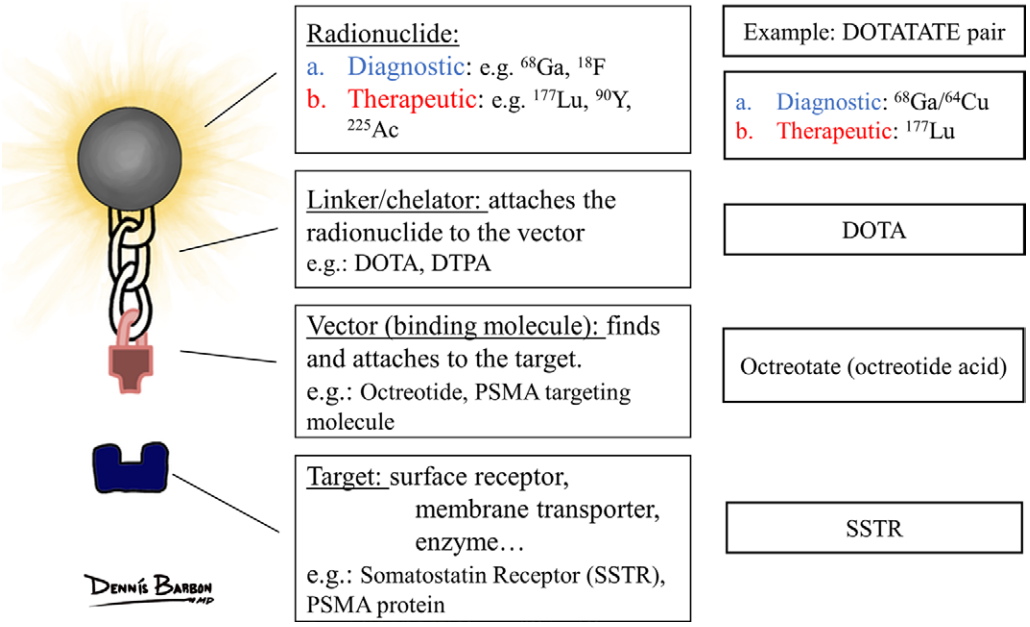

Figure 6. Diagram illustrates the concept of theranostic agents. The same molecular target is used for imaging and treatment of a specific biologic process. For imaging purposes, the agent can be labeled with a γ or β-plus emitter; for targeted therapy, it can be labeled with a β-minus or α emitter. An example is the structure of ^{177}Lu-DOTATATE used to treat well-differentiated neuroendocrine tumors. *DOTA* = 1,4,7,10-tetraazacyclododecane-1,4,7,10–tetraacetic acid, *DTPA* = diethylenetriaminepentaacetic acid, *PSMA* = prostate-specific membrane antigen.

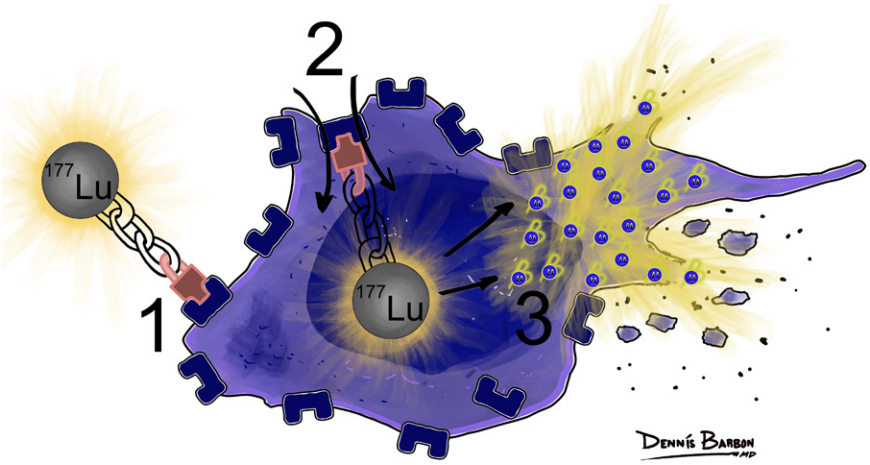

Figure 7. Mechanism of action of ^{177}Lu-DOTATATE. *1.* The complex binds to somatostatin receptors overexpressed on the surface of well-differentiated neuroendocrine tumors. *2.* The complex is internalized. *3.* Beta-minus particles emitted from the complex cause DNA breaks and cell death.

presence of the cancer stem cells phenotype, which is linked to aggressive behavior (19). In addition, radiation may induce both immunosuppressive and immunostimulatory effects in the tumor microenvironment; this change in the local immune response can enhance or limit the efficacy of the therapy (19,20).

Toxicity is an important consideration with RPT, and it is essential to remember that not all organs are affected equally by radiation. Cells dividing rapidly are thought to be more vulnerable to radiation. The International Commission on Radiological Protection (ICRP) compiles tissue-weighting factors (W_T's) to account for these differences. For example, bone marrow is a very radiosensitive organ (W_T = 0.12), while the brain is more radioresistant (W_T = 0.01) (21). Additionally, patient-specific factors such as prior therapies and comorbidities may predispose a patient to developing side effects from the RPT; for example, a history of prior chemotherapy with alkylating agents has been described as a potential risk factor for development of myelodysplastic syndrome and acute leukemia after RPT for neuroendocrine tumors (22–24). These risk factors, which dictate patient-specific susceptibility to develop toxic effects from RPTs, remain poorly understood and are the topic of active research.

In addition to these tumor- and patient- or organ-related factors, there are therapy-related factors that affect both the therapeutic effect and the organ toxicity.

Type of Radiation Emitted and Its Energy

Owing to their short range and high LET, α particles are more effective at cell killing, with fewer side effects in the surrounding normal tissue. The ability of targeted α therapy to overcome treatment resistance to β particle therapy in metastatic PSMA-positive castration-resistant prostate cancer and in metastatic somatostatin receptor–positive neuroendocrine tumors has recently been described, promoting further research in this new direction (25,26).

In contrast, β-minus particles have much lower LET over greater path lengths. Although this may lead to greater toxic effects on neighboring tissues, it simultaneously carries a clinical advantage, called the *cross-fire effect*. The longer

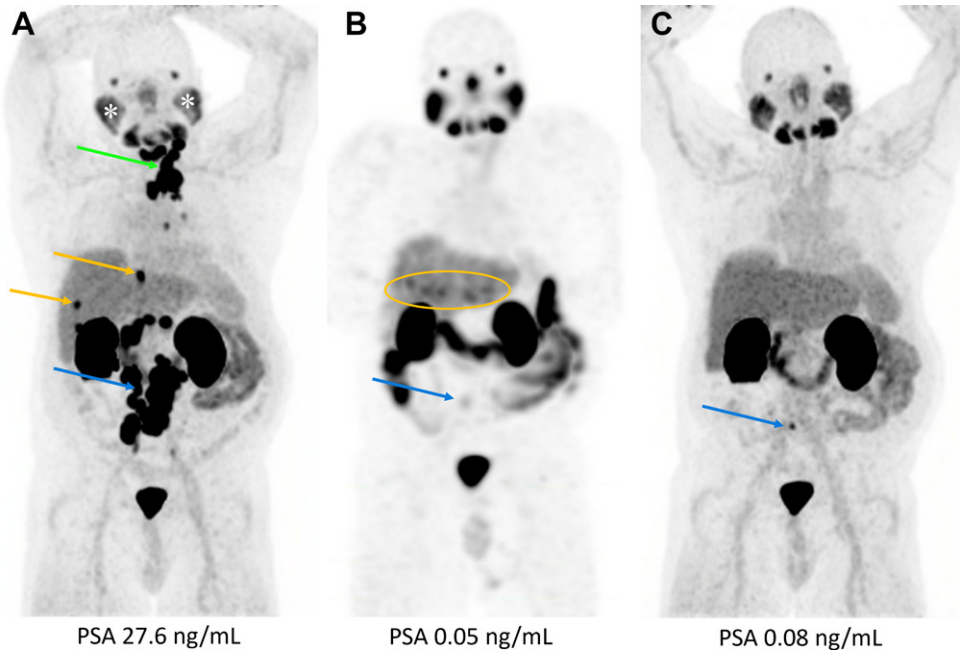

Figure 8. RPT with ^{177}Lu–prostate-specific membrane antigen (PSMA)-617 in a 77-year-old man with metastatic castration-resistant prostate cancer. *PSA* = prostate-specific antigen. **(A)** Coronal maximum intensity projection (MIP) image from PSMA PET/CT using the PSMA targeting agent ^{18}F-DCFPyL (^{18}F-piflufolastat) performed to determine eligibility for treatment shows intense uptake in retroperitoneal (blue arrow), mediastinal, and left supraclavicular (green arrow) lymphadenopathy, as well as in two metastatic liver lesions (yellow arrows). Note the physiologic distribution of the radiopharmaceutical, including significant uptake in the salivary and lacrimal glands, mild uptake in the background liver parenchyma, and excretion in the urinary system. The salivary gland uptake of PSMA-targeting radioligands is responsible for the xerostomia, which is a common side effect of RPT with these agents. Tumor uptake (maximum standardized uptake value [SUV_{max}] = 32) is higher than parotid gland uptake (*). These results confirmed the patient's eligibility for treatment. After the first two cycles of RPT, the PSA level dropped significantly. **(B)** Coronal MIP image from posttherapy SPECT/CT performed 24 hours after the second cycle of ^{177}Lu–PSMA-617 (using the γ emissions of ^{177}Lu) shows significant tumor response, with minimal residual uptake in a retroperitoneal node (arrow). Mild heterogeneous uptake in the liver (yellow oval) with no correlate at contrast-enhanced CT (not shown) was thought to be artifactual. Note the physiologic excretion in the colon at 24 hours after therapy. **(C)** Coronal MIP image from repeat PSMA PET/CT with ^{18}F-DCFPyL performed to confirm the findings shows residual uptake in a small retroperitoneal lymph node (arrow). The additional lymphadenopathy and liver metastases seen at pretherapy PET have resolved. Note that the level of uptake is not directly comparable between the SPECT and PET images due to the difference in sensitivity and resolution between the two modalities; more intense uptake is expected at PET. Given the residual uptake in the retroperitoneal node seen at PET, the patient continued to receive the remaining cycles of the therapy, with stable disease subsequently.

Table 2: Most Common Clinically Used Theranostic Pairs

Pathologic Condition	Theranostic Pair		Target or Mechanism of Action	Emission	Imaging
Metastatic castration-resistant prostate cancer	Diagnostic	^{18}F-DCFPyL ^{68}Ga–PSMA-11	PSMA	β plus	PET
	Therapeutic	^{177}Lu–PSMA-617		β minus or γ	SPECT or planar
Neuroendocrine tumor	Diagnostic	^{64}Cu- or ^{68}Ga-DOTATATE	Somatostatin receptors (SSTRs)	β plus	PET
	Therapeutic	^{177}Lu-DOTATATE		β minus or γ	SPECT or planar
Thyroid cancer	Diagnostic	^{123}I-NaI	Sodium/iodide symporter (NIS)	Electron capture	SPECT or planar
	Therapeutic	^{131}I-NaI		β minus or γ	SPECT or planar
Pheochromocytoma and paraganglioma	Diagnostic	^{123}I-MIBG	Norepinephrine analog	Electron capture	SPECT or planar
	Therapeutic	^{131}I-MIBG		β minus or γ	SPECT or planar
Liver malignancies	Diagnostic	^{99m}Tc-MAA	Takes advantage of tumor hypervascularity	γ	SPECT or planar
	Therapeutic	^{90}Y-microsphere		β minus or β plus*	SPECT (bremsstrahlung) or PET
Bone metastases from prostate cancer	Diagnostic	^{99m}Tc-MDP	Chemisorption	γ	SPECT or planar
	Therapeutic	^{223}Ra-dichloride	Calcium analog	α	N/A

Note.—DCFPyL = piflufolastat, MAA = macroaggregated albumin, MDP = methylene diphosphonate, N/A = not applicable, ^{99m}Tc = technetium 99m (metastable).
* A small amount of internal pair production results in β-plus particles used for PET imaging.

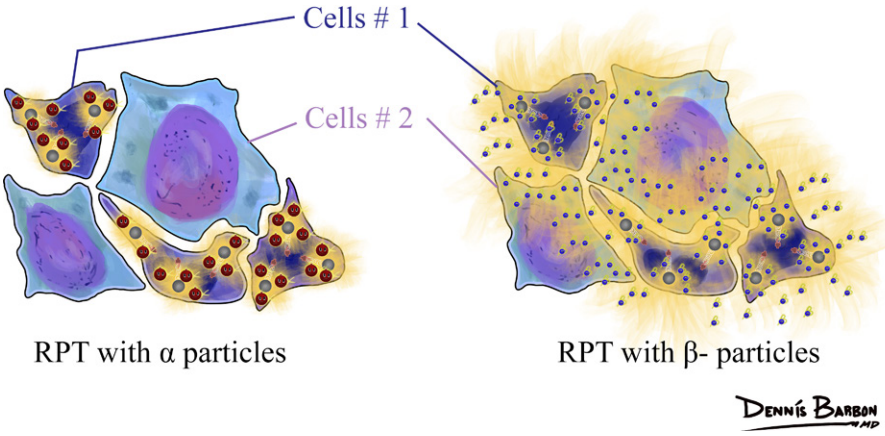

Figure 9. Alpha particles have a short range and deliver localized damage. In contrast, β-minus particles have a greater path length, which allows irradiation of tumor cells that do not express the molecular target *(cells #2)* from cells that do express the target and concentrate the therapeutic agent *(cells #1)*. This is known as the cross-fire effect and is thought to be an advantage of β-minus particles for RPT in heterogeneous tumors.

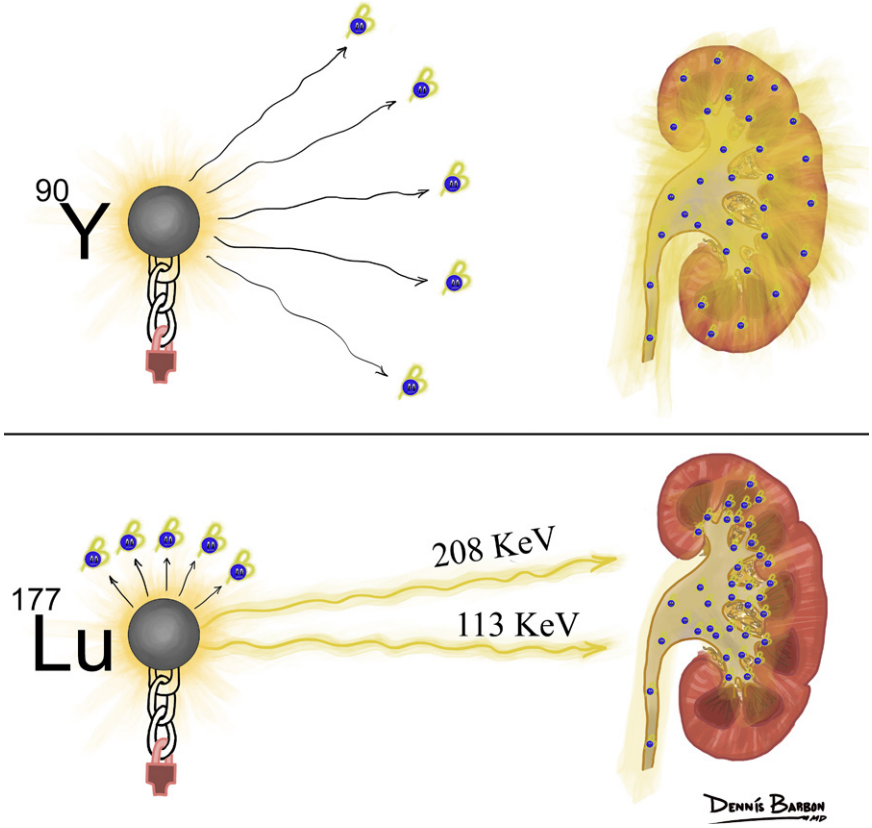

Figure 10. The β-minus particle of ^{90}Y has higher energy relative to that of ^{177}Lu and therefore a longer range in tissue. This is thought to be responsible for the higher rate of renal toxicity observed with RPT in neuroendocrine tumors using ^{90}Y. With both ^{90}Y- and ^{177}Lu-labeled somatostatin agonists, an amino acid solution is infused along with the therapy to reduce the proximal tubular reabsorption of the radiopharmaceutical and therefore reduce the risk of renal toxicity. Note that ^{177}Lu emits additional γ radiation (energies of 208 and 113 keV).

Table 3: Characteristics of ^{90}Y and ^{177}Lu

Radionuclide	^{90}Y	^{177}Lu
Half-life (d)	2.7	6.7
Average energy of emitted β-minus radiation (keV)	935	133
Maximum range of emitted β-minus radiation (mm)	12	2
Energy of γ emission (keV)	NA*	113, 208

* NA = not applicable.

range of the β particle allows irradiation of tumor cells that are difficult to reach by the therapeutic agent from cells that demonstrate uptake of the agent (Fig 9) (27).

Additionally, not all β emitters are the same. The β-minus particles emitted by two of our most commonly used β-minus radionuclides, ^{177}Lu and ^{90}Y, have different physical decay characteristics that carry clinical implications. For example, the higher energy—which leads to a longer range in tissue—of the β-minus particle emission from ^{90}Y compared to that from ^{177}Lu is thought to be responsible for the higher rate of renal toxicity observed with RPT using ^{90}Y- versus ^{177}Lu-labeled somatostatin agonists (Fig 10) (23,28). However, this longer tissue path length is thought to be advantageous for ^{90}Y in treating larger tumors or tumors with heterogeneous uptake (Table 3).

Effective Half-life and Agent Retention

The physical half-life is the time it takes the radionuclide to decay to half of its initial activity. The biologic half-life is the time

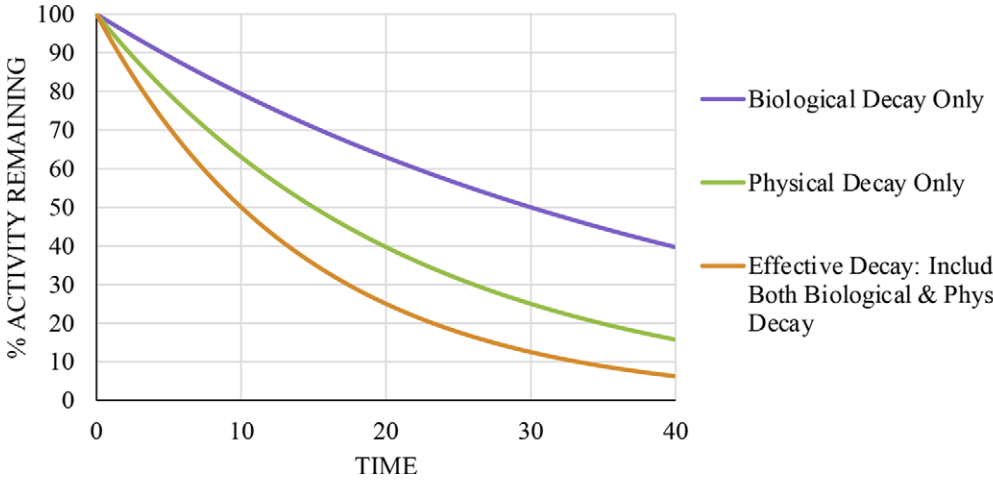

Figure 11. Relationship between the physical (T_p), biologic (T_b), and effective (T_e) half-lives. The effective half-life accounts for both physical decay and biologic clearance. Therefore, it is shorter than both the biologic and physical half-lives, bound by the following formula: $T_e^{-1} = T_p^{-1} + T_b^{-1}$.

Table 4: PSMA Expression Score and Eligibility for RPT according to the PROMISE V2 Criteria

Score	Uptake Relative to Internal Reference	Eligibility for RPT
0	≤Blood pool	No
1	≤Liver and > blood pool	No
2	≤Parotid gland and > liver	Yes
3	>Parotid gland	Yes

Source.—Reference 33.

needed to eliminate half of the administered agent based on only biologic clearance. The effective half-life is the time it takes for half of the radiotracer activity to clear from the body, accounting for both physical and biologic decay (and is therefore shorter than both the biologic and physical half-lives) (Fig 11).

The longer the agent retention in a certain tissue, the higher the expected damage to this tissue (tumor or normal organ). For example, the longer the radiotracer circulates in the blood, the greater the risk of radiation toxicity to the bone marrow. For the same administered activity, slower clearance will lead to longer biologic half-life and higher bone marrow toxicity (29,30).

Administered Activity

Higher administered activity may result in greater therapeutic effect on the target lesions, but may also be accompanied by greater toxicity risk to organs at risk and off-target tissues. When significant toxicity occurs, it is recommended to temporarily or permanently withhold treatment—depending on the grade of the toxicity—to allow recovery of organ function. If this function improves, allowing the patient to proceed with the treatment, it is typically recommended to administer a reduced dose for the subsequent cycles, to reduce the likelihood of recurrent toxicity. The protocols followed to manage side effects vary by type of RPT (Fig S3) (2,3).

Agent Distribution

The distribution and degree of uptake of the therapeutic agent in tissue will contribute to tissue damage and therefore to both the antitumor therapeutic effect as well as organ toxicity. Tumor expression of the target is required for targeted treatment (Table 4), and a high level of uptake in tumors is predictive of a higher therapeutic response, as discussed in detail later (28,31–33). Similarly, organs with high physiologic uptake are at higher risk for radiation toxic effects. For example, dry mouth (xerostomia) is a common side effect from ^{177}Lu-PSMA therapies, observed in 38.8% of patients who received the therapy in the VISION trial (Fig 12) (13,28).

Dosimetry

Radiation dosimetry is of growing interest in nuclear medicine and theranostics, especially to personalize RPT to individual patients. Fundamentally, the radiation dose is the energy imparted by ionizing radiation per unit mass of tissue, measured in units of gray (Gy) (6). The absorbed dose to tissue is a common metric for assessing the safety and radiation risk of both diagnostic and therapeutic applications of ionizing radiation.

While individualized dosimetry calculations are standard practice for patients undergoing external-beam radiation therapy (EBRT), RPTs are typically administered as a fixed treatment activity (34,35). However, the rationale for dosimetry remains the same: that patient-specific estimates of dosimetry can help maximize therapeutic effect while mitigating potential radiation-related toxicity. Until recently, dosimetry was rarely performed for RPT, but interest and research in this domain are growing, and there is an increasing body of evidence showing correlation between absorbed dose and both treatment efficacy and side effect profile (36,37).

Framework for Dose Calculations

To estimate the dose absorbed to a target tissue from an unsealed radiation source (ie, injected into the bloodstream, or not sealed in any container, such as an infusion of RPT), it is useful to define a target-and-source framework (6). A *source* is any defined region that accumulates activity, while a *target* is the organ or tissue receiving radiation, for which the dose is being calculated. Any source region can also be the target region itself and thereby self-irradiate. These regions can be of any size, depending on the application, from whole organs

Figure 12. Agent distribution in an 83-year-old man with metastatic castration-resistant prostate cancer referred for consideration of ^{177}Lu–PSMA-617 therapy. Coronal MIP image from ^{18}F-DCFPyL PET/CT shows intense PSMA expression at the sites of disease, including the prostate bed (blue arrow), left hilar and retroperitoneal lymph nodes (yellow arrow and oval, respectively), and diffuse osseous lesions (green arrows = representative metastases in the ribs and right acetabulum). The tumor uptake is higher than in the parotid gland (score = 3), with maximum standardized uptake value (SUV_{max}) of 34, predictive of good response to therapy. Note the intense uptake in the salivary glands (∗). Xerostomia is a common side effect with this therapy, with no proven approach to minimize the salivary gland toxicity. In patients with symptomatic dry mouth, lubricating rinses may help.

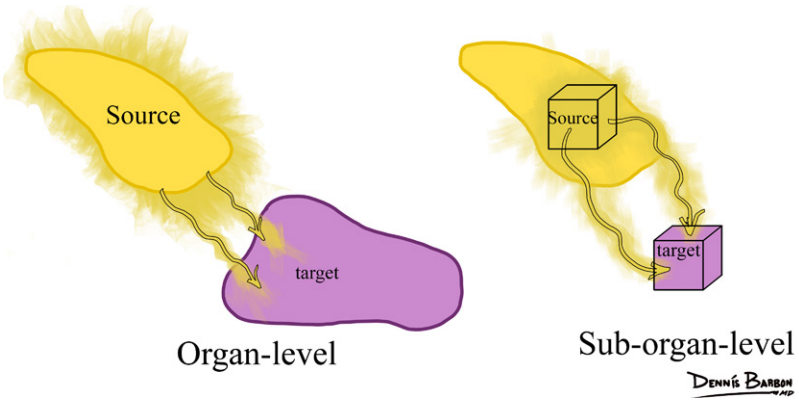

Figure 13. The Medical Internal Radiation Dose (MIRD) schema defines a source-and-target framework for estimating radiation dose. The source is any region that accumulates activity, and the target is the recipient of radiation from any other source. Organ-based methods for dosimetry assume a uniform distribution of activity in the organs and do not usually account for patient-specific anatomy. They approximate dose delivery from one organ to another based on computational phantoms. Sub–organ-level dosimetry accounts for patient-specific nonuniform activity distributions within organs and tumors. It allows calculation of absorbed doses using voxel-level dose factors or isotope spatial distribution models, which account for more clinically accurate heterogeneous distribution.

and tumors to organ subregions to individual voxels or even cells. Hence, this framework provides flexibility with respect to the scale of the dose estimates (Fig 13).

To quantify the total absorbed energy in a region, it is crucial to estimate both the total cumulative number of emissions in each source region (the cumulated activity) and the energy imparted per decay. The absorbed dose is also intimately related to the spatial path length of the particle emissions. The absorbed fraction describes the fraction of emissions emitted in a source region that are absorbed by a neighboring target region. The total dose to a target region is the summation of all dose contributions from individual sources.

Patient-specific Factors

Given that the RPT distributes in the patient over time and that it is removed by both physical decay and biologic washout processes, estimation of the cumulated activity is necessarily a kinetic problem. Therefore, the dose will not only depend on the decay properties of the radioisotope, but also on the pharmacokinetics and retention of the RPT as well as patient-specific biokinetics (eg, the patient's renal function). One example where patient-specific factors can have a significant effect on the absorbed dose is treatment with ^{131}I-NaI for thyroid cancer. While this treatment is often prescribed at standard empirical doses ranging from 75 to 200 mCi (2775 to 7400 MBq), different RPT clearance rates can lead to bone marrow toxicity even in the empirical activity range.

As shown in Figure 14, patient-specific dosimetry workflows can be used to measure activity concentration in serial blood samples and whole-body counts to model ^{131}I-NaI clearance, to estimate the maximum tolerable activity while limiting the bone marrow dose to less than the accepted dose limit of 2 Gy (38,39). The administered treatment activity is optimized for each patient to limit the bone marrow dose, depending on the clearance kinetics and relative retention.

Molecular Imaging for Dosimetry

The accumulation of the given radiopharmaceutical will depend on both the intensity and heterogeneity of target expression in the tumor and normal organs, as well as the radiopharmaceutical biokinetic profile (36). Molecular imaging is used to help identify the biodistribution of the radiopharmaceutical activity in each patient over the course of the treatment. While there are different approaches to imaging therapeutic radiopharmaceutical distribution (SPECT, planar imaging, or hybrid imaging), for best quantitative accuracy, it is recommended to perform quantitative SPECT/CT (40). Optimal time sampling will depend on the uptake and clearance kinetics of the specific RPT agent, but it is common practice to acquire a minimum of three time points of SPECT after treatment (41,42). These images can then be used to segment

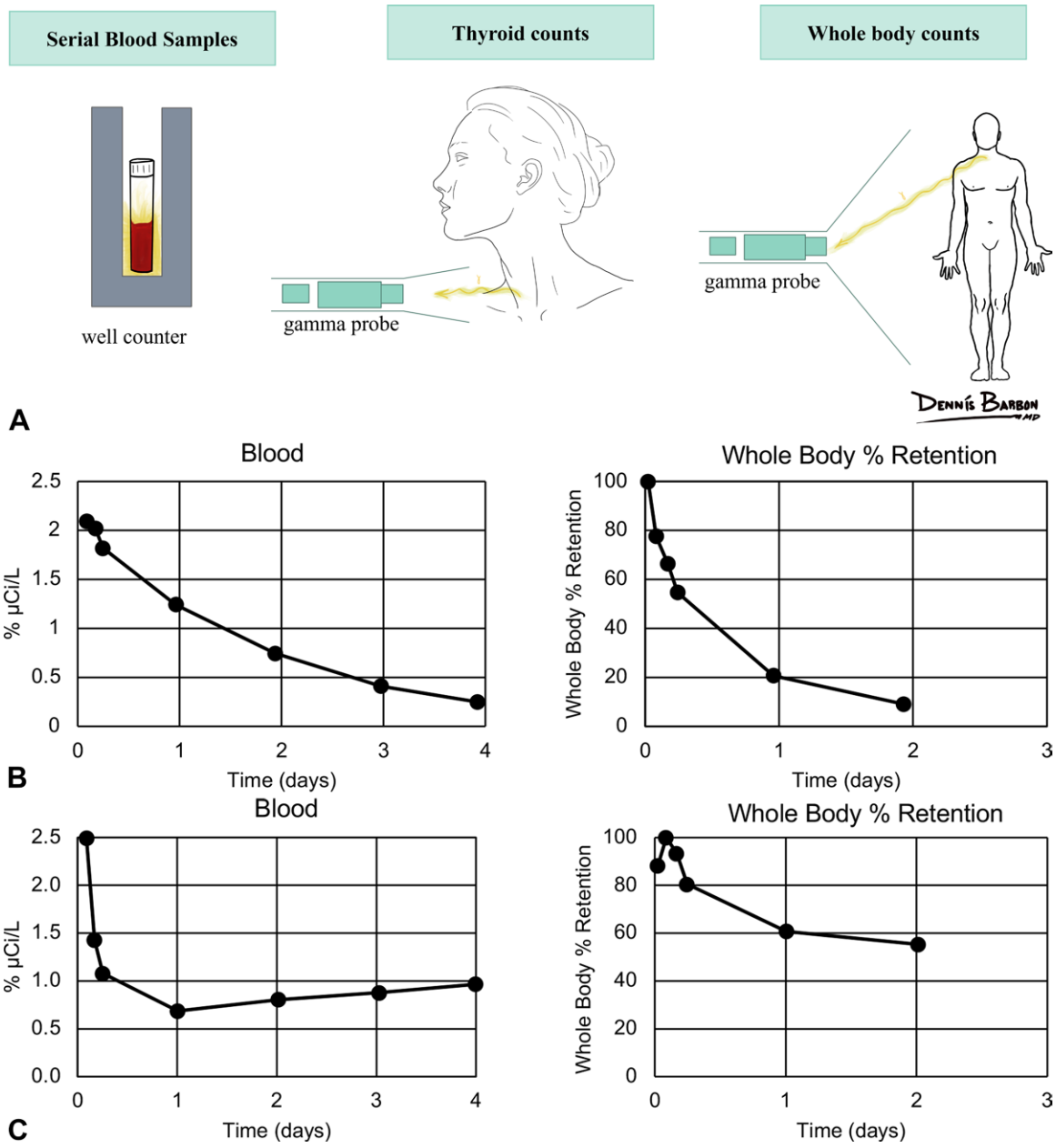

Figure 14. Patient-specific dosimetry of ^{131}I-NaI for treatment of thyroid cancer (or blood dosimetry). **(A)** After administration of a subtherapeutic activity of ^{131}I-NaI, a well counter is used to measure activity in serial blood draws, and a γ probe is used to detect whole-body and thyroid counts. **(B, C)** The blood curves are generated by measuring the radioactivity in blood samples and removing the effects of physical decay, while the whole-body percentage retention of the ^{131}I-NaI is expressed as fractional retention based on external exposure measurements obtained from the γ probe counts. The uptake and clearance curves are analyzed to calculate the maximum tolerable activity, while limiting bone marrow dose to the accepted limit of 2 Gy. **(B)** Representative time-activity curves for blood and whole-body counts for a patient exhibiting rapid clearance kinetics show that higher treatment activity could be tolerated without exceeding the dose limit to the bone marrow. In this patient, the maximum tolerable dose was 348 mCi (12 876 MBq), well above the empirical dose of 200 mCi (7400 MBq). **(C)** Representative time-activity curves for blood and whole-body counts for a patient exhibiting prolonged retention of ^{131}I-NaI, where the dose limit to the bone marrow would be exceeded without an activity reduction. In this patient, the maximum tolerable dose was 130 mCi (4810 MBq), well below the empirical dose.

regions of interest, where the exact organs at risk will be determined by the therapy.

Given that these images capture a snapshot in time of the activity concentration and spatial distribution of the radiopharmaceutical, we can then generate a time-activity curve for every region of interest, which describes how the activity is accumulated, distributed, and excreted by a region over the time course of the treatment. The area under the curve defines the cumulated activity, which can then be multiplied by the energy per decay and the absorbed fraction for the specific source and

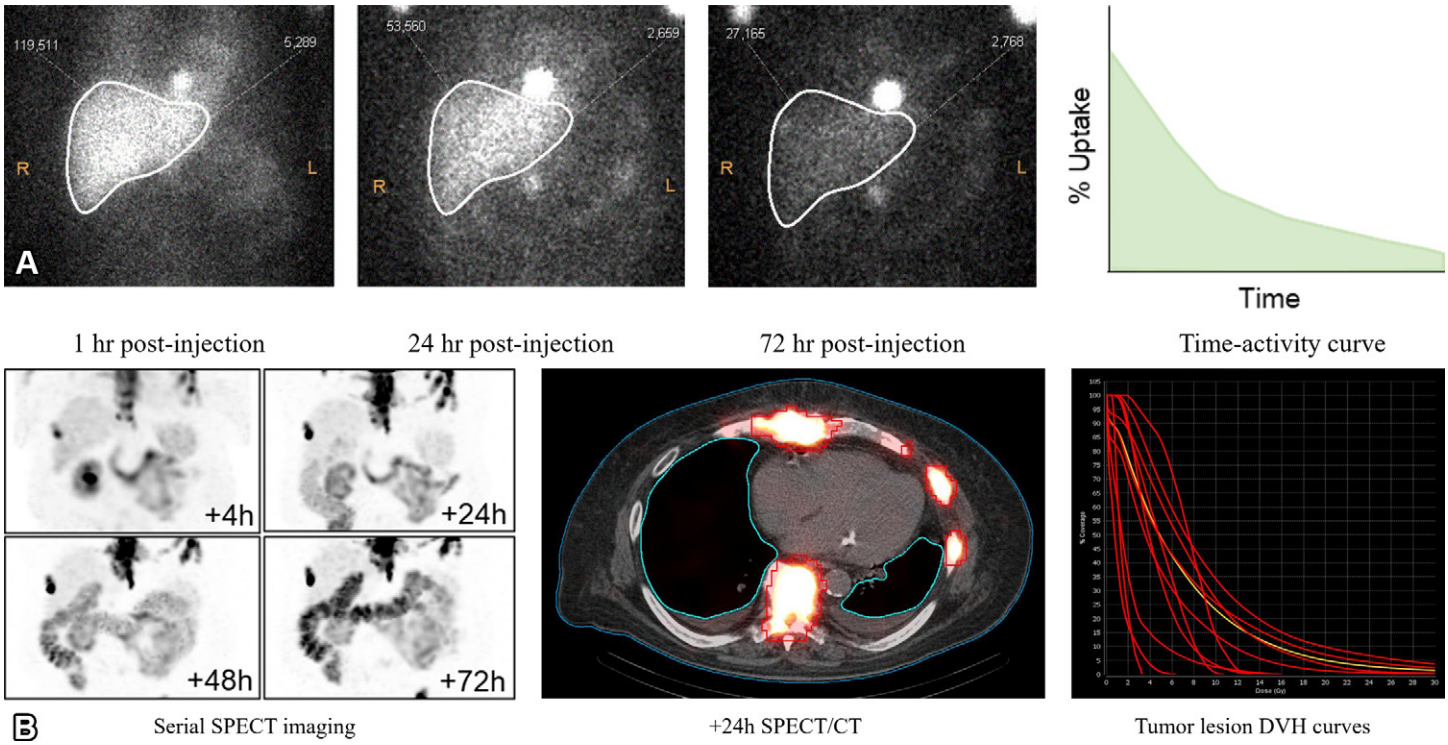

Figure 15. Examples of organ-level **(A)** and lesion-level **(B)** dosimetry. **(A)** Organ-level dosimetry in a patient with metastatic pheochromocytoma referred for treatment with high-specific-activity ^{131}I-MIBG. Pretreatment dosimetry consisted of serial planar scans performed after administration of a small dose (5 mCi or 185 MBq) of ^{131}I-MIBG. Liver contours are displayed. The mean counts in the liver region are used to generate a time-activity curve, from which the total cumulated activity can be derived. The same process is repeated for the lungs and kidneys to compare mean absorbed doses against established organ dose limits. *hr* = hour. **(B)** Lesion-level dosimetry in a patient with metastatic castration-resistant prostate cancer. Serial quantitative SPECT/CT scans were performed after ^{177}Lu–PSMA-617 therapy. The counts in each voxel of the contoured area are used to estimate the cumulated activity distribution on a voxel level; in this example, the bone lesions are contoured in red and the lungs are contoured in blue. Dose-volume histograms *(DVHs)* can be used to display and analyze the dose distribution within the contoured region of interest. This allows calculation of the absorbed dose in the area of interest, which may be a tumor or an organ at risk. *h* = hour, *MIP* = maximum intensity projection.

target to determine the absorbed dose. The absorbed dose per cumulated activity is known as an *S factor* and represents a radiation transport factor that is unique to the source and target. For normal organs, these factors are often tabulated based on particle transport simulations and typically used for estimations of population-level dose and risk assessments.

Voxelwise Dosimetry

Importantly, organ-level dosimetry approximates dose absorption, assuming a uniform distribution of activity in the organs (and tumors). Sub–organ-level dosimetry (eg, on the voxel scale) accounts for patient-specific nonuniform activity distributions within organs and tumors.

For voxelwise dosimetry, energy deposition is generally calculated by transforming the three-dimensional activity distribution into a dose distribution using outputs from particle simulations, thereby modeling the heterogeneous radiopharmaceutical distribution observed within organs and tumors. Figure 15 depicts different examples of dosimetry in clinical practice: organ-level dosimetry using planar scans for ^{131}I-MIBG organ dose estimates (Fig 15A) and voxelized lesion dosimetry for ^{177}Lu–PSMA-617 based on serial quantitative SPECT/CT scans (Fig 15B). Lesion dosimetry is also integrated into dose planning and verification for ^{90}Y microsphere radioembolization. In this case, a planning ^{99m}Tc-MAA (macroaggregated albumin) SPECT/CT scan is performed as a surrogate to estimate target tumor dose and extrahepatic shunting from ^{90}Y microsphere radioembolization. Posttherapy imaging can be performed with ^{90}Y bremsstrahlung SPECT or PET to assess the actual delivered dose and microsphere biodistribution.

Clinical Implementation of Dosimetry

One important practical consideration is implementation of dosimetry in clinical practice. While individualized dosimetry provides another dimension of patient-specific evaluation, the labor-intensive requirements of dosimetry and lack of standardization have thus far precluded widespread adoption. In particular, dosimetry can be difficult to accommodate from the perspective of both the clinic and the patient, especially if patients are returning for imaging over multiple days.

For dosimetry to be more broadly adopted, support must be given to studies investigating the relationship between dose and response, as well as those studying treatment with patient-specific treatment activities, including through clinical trials incorporating dosimetry. It is also necessary for the field to provide guidance regarding standardization of dosimetry methods to ensure consistent reproducible dose

Table 5: Criteria for Release and Need for Instructions after RPT with ^{131}I according to the NRC* Guide

Criteria for Release	Need for Instructions
Administered or retained activity ≤ 33 mCi (1221 MBq)	Administered or retained activity > 7 mCi (259 MBq)
Measured dose rate at 1 m ≤ 0.07 mSv/h (7 mrem/h)	Measured dose rate at 1 m > 0.02 mSv/h (2 mrem/h)
Calculated bystander dose ≤ 5 mSv (0.5 rem)	Calculated bystander dose > 1 mSv (0.1 rem)

* NRC = Nuclear Regulatory Commission.

estimates across institutions and users. Several guidance documents are available from the Society of Nuclear Medicine and Molecular Imaging (SNMMI) and European Association of Nuclear Medicine (EANM) to aid practitioners in establishing a dosimetry practice for ^{177}Lu-labeled RPT agents (40,43). Continued harmonization of dosimetry methods remains a priority focus area for nuclear medicine and physics professional societies.

Multiple dosimetry software tools are now both freely and commercially available and can be integrated with the image processing workflows to aid with dose estimations. In addition, the development of automated segmentation algorithms may reduce the time spent on manual segmentation of regions of interest. Furthermore, other efforts focused on simplification of dosimetry include investigating the potential for dose estimates based on a single time point of posttherapy imaging (44–46). Therein lies an important burgeoning role for nuclear medicine physicists, who can aid in development of clinical imaging protocols, image quantification, and of course calculations of patient-specific dosimetry. With the emergence of these dosimetry softwares and advanced tools to ease clinical implementation, dosimetry is becoming increasingly accessible to meet the growing demand for a more personalized treatment paradigm.

Posttherapy Radiation Safety

Safety precautions are often needed after RPT to minimize radiation exposure to the patient's environment. According to the U.S. Nuclear Regulatory Commission (NRC) guidelines, a licensee may authorize release from its control of any individual who has been administered radiopharmaceuticals "if the total effective dose equivalent to any other individual from exposure to the released individual is not likely to exceed 5 mSv (0.5 rem)" (47). Released individuals frequently require radiation safety instructions for the days after the treatment.

The strictness and duration of the precautions needed depend on multiple therapy- and patient-dependent factors, such as the type of radiation emitted and its energy. More stringent precautions are needed with higher γ fractions and γ energy emissions (given their longer range); as such, therapeutic radionuclides that also emit γ (eg, ^{131}I and ^{177}Lu) require more radiation safety precautions relative to pure β or α emitters (eg, ^{90}Y or ^{223}Ra). Higher administered activities and longer effective half-life or agent retention lead to higher radiation exposure to the patient's environment, and occasionally patients treated with high activities may need admission in a shielded room until they meet release criteria.

In addition to the patient distancing from others, the radiotracer's excretion route may require additional precautions. For example, radiotracers with urinary excretion, such as ^{177}Lu–PSMA-617 (2), require bathroom hygiene and appropriate handling of urinary contaminations, while radiotracers with fecal excretion, such as ^{223}Ra-dichloride (48), require appropriate handling of material contaminated by feces.

A regulatory guide by the NRC provides detailed guidance on methods acceptable to determine the need for posttherapy instructions as well as the release criteria after RPT, which can be based on the administered activity, measured dose rate, or patient-specific dose calculation (49) (Table 5).

Tumor Heterogeneity

Tumor heterogeneity describes the presence of different phenotypes within the same (intra-) or across different (inter-) tumors. This can reflect either tumor size and metabolic dynamics (eg, development of a hypoxic or necrotic core in a poorly vascularized mass) or molecular (genetic and nongenetic) heterogeneity (50,51). Increased mutations and development of unique subclones of the tumor population is generally more concerning for morbidity, as each additional mutation presents a chance for increased grade or drug resistance (52). Greater heterogeneity within the original tumor presents more opportunities for an initially resistant subclone to be present and correlates with worse prognosis (53). Treatment imposes a selection pressure that can subsequently lead to domination of the resistant subclones (Fig 16).

At anatomic imaging, heterogeneity can manifest through physical differences such as overall size and morphology of the tumor (eg, necrosis, margins, degree of enhancement), as well as differences in response to treatment between different lesions (54,55). However, these physical characteristics are not well correlated with particular molecular characteristics. In contrast, molecular imaging allows evaluation of the expression of specific molecular targets, their distribution throughout the body, their degree of expression, and the dynamic changes of these features over time. With PET, standardized uptake values (SUVs), also referred to as conventional PET metrics, are routinely used to quantify target expression, reflected by the degree of tumor uptake. Radiomics and textural analysis may provide better evaluation of tumor heterogeneity (56). Analysis of textural parameters with somatostatin receptor and PSMA PET has shown improved prognostic value as compared with analysis of SUV alone (57–59).

Tumor heterogeneity is a well-documented phenomenon in both neuroendocrine tumors and prostate cancer (60–62). This heterogeneity exists on multiple levels: interindividual, which is observed between patients with the same type of tumor (Fig 17) (63), and intraindividual, which occurs within a single patient. Intraindividual heterogeneity can be further classified as either spatial or temporal. Spatial heterogeneity can manifest in two ways: interlesional, seen as variations between different lesions within the same individual (Fig 18), or intralesional, seen as variations within a

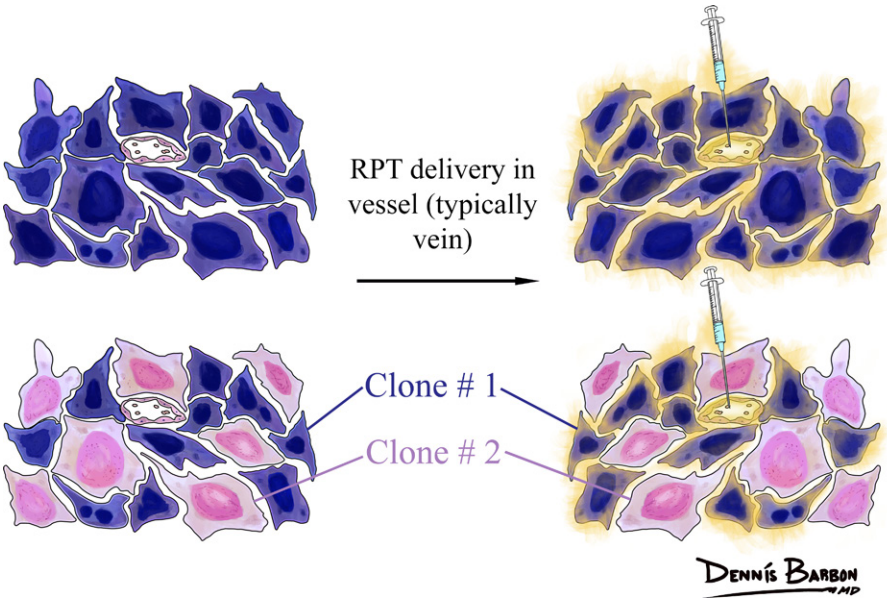

Figure 16. Top: In a homogeneous tumor, cells receive radiation in a somewhat homogeneous way with RPT. Bottom: In a heterogeneous tumor, cells expressing the target receive the therapeutic agent *(clone #1)*, while cells that lack target expression do not *(clone #2)*.

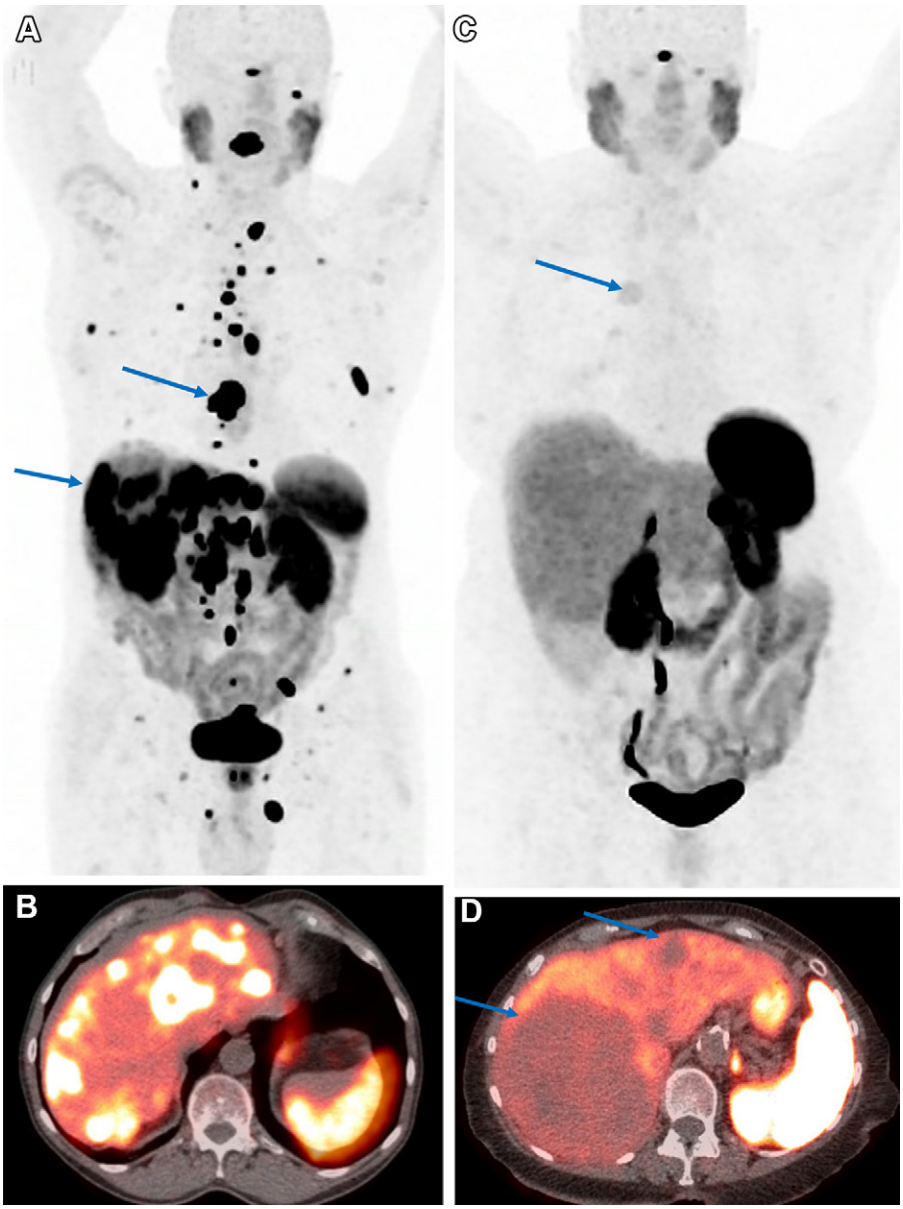

Figure 17. Interindividual tumor heterogeneity in two patients with metastatic neuroendocrine tumors, both with well-differentiated World Health Organization (WHO) grade 2 tumors, imaged with ^{64}Cu-DOTATATE PET/CT. **(A, B)** In a 72-year-old man with a small-bowel primary tumor, coronal MIP **(A)** and axial **(B)** PET/CT images show intense DOTATATE uptake in hepatic and osseous metastases (arrows in **A**) (tumor uptake greater than that of background liver), indicating high somatostatin receptor expression in the tumor. **(C, D)** In an 83-year-old woman with a pancreatic primary tumor, coronal MIP **(C)** and axial **(D)** PET/CT images show faint DOTATATE uptake in hepatic and osseous metastases (arrows) (tumor uptake less than that of background liver), indicating lack of sufficient somatostatin receptor expression.

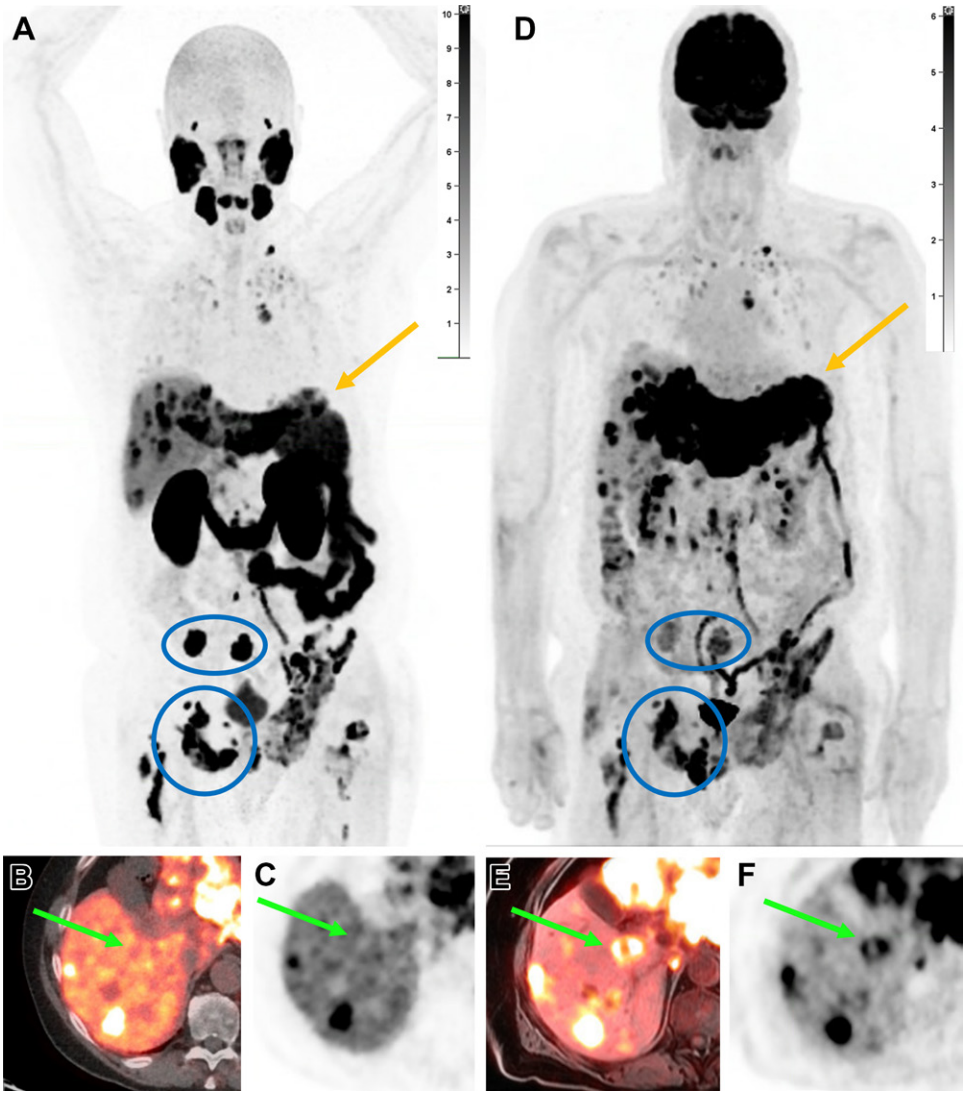

Figure 18. Intraindividual tumor heterogeneity in a 78-year-old man with progressing metastatic castration-resistant prostate cancer previously treated with hormonal therapy and docetaxel, who was referred for consideration of ^{177}Lu–PSMA-617 therapy. ^{18}F-DCFPyL PET/CT was performed to assess eligibility for treatment. **(A–C)** Coronal MIP **(A)**, axial PET/CT **(B)**, and axial PET **(C)** images show increased PSMA uptake in metastatic disease to the bones, liver, lungs, and supraclavicular nodes. However, several liver lesions are photopenic (arrow in **B** and **C**), concerning for PSMA-negative disease, which prompted evaluation with ^{18}F–fluorodeoxyglucose (FDG) PET. **(D–F)** Coronal MIP **(D)**, axial PET/MRI **(E)**, and axial PET **(F)** images from ^{18}F-FDG PET/MRI performed 1 month later show FDG uptake in the PSMA-negative liver lesions (arrow in **E** and **F**), in keeping with discordant FDG-avid PSMA-negative disease, concerning for more aggressive disease. Note the enlargement of the left hepatic lobe from quick progression of hypermetabolic metastases (arrow in **A** and **D**). The bone metastases show more intense uptake with PSMA than with FDG (blue circle and oval in **A** and **D**). On the basis of these findings, the patient was not considered a suitable candidate for RPT and was considered for second-line chemotherapy instead.

single lesion. Temporal heterogeneity refers to changes over time, including the development of higher-grade disease (Fig 19). The latter is important to track in therapy response, as loss of target expression in new or growing lesions may indicate development of dedifferentiated subclones (64).

Although tissue sampling allows evaluation on a cellular level, which is below the resolution of imaging, it analyzes a small core of one particular lesion and carries the risk of sampling error (Fig 20). Molecular imaging provides the unique opportunity to noninvasively evaluate macroscopic tumor heterogeneity throughout the body (interlesion heterogeneity) and over time (temporal heterogeneity) (61,62).

Implications of Tumor Heterogeneity

Eligibility for RPT depends on adequate expression of the molecular target. Imaging is the cornerstone of assessing for this target expression, which is referred to as a "treat what you see" paradigm. Eligibility criteria may differ between trials, even for the same molecular target. For ^{177}Lu-DOTATATE and ^{177}Lu–PSMA-617, eligibility was defined as visual tumor uptake above background liver, per the clinical trials that led to the U.S. Food and Drug Administration approval of these therapies: the NETTER-1 trial (65) and the VISION trial (13), respectively.

In the VISION trial, patients with PSMA-negative lesions were excluded to ensure that no significant lesions (that do not express the target) would remain untreated. PSMA-negative lesions were defined as those with uptake less than or equal to that of liver parenchyma in *(a)* any lymph node with a short axis greater than or equal to 2.5 cm or *(b)* any metastatic solid-organ lesion or bone lesion with a soft-tissue component and a short axis greater than or equal to 1.0 cm (Fig 21).

More than one therapeutic option can be available for certain tumors, and imaging can help determine which option is most appropriate. Pheochromocytoma and paraganglioma are a perfect illustration of this concept, with two potential targets: *(a)* norepinephrine transporter theranostic pair ^{123}I-MIBG and high-specific-activity ^{131}I-MIBG (66) and *(b)* somatostatin receptor theranostic pair ^{68}Ga- or ^{64}Cu-DOTATATE and ^{177}Lu-DOTATATE) (67). When RPT is considered for unresectable or metastatic pheochromocytoma or paraganglioma, tumor uptake with both imaging agents should be considered in guiding the choice of RPT (Fig 22) (68).

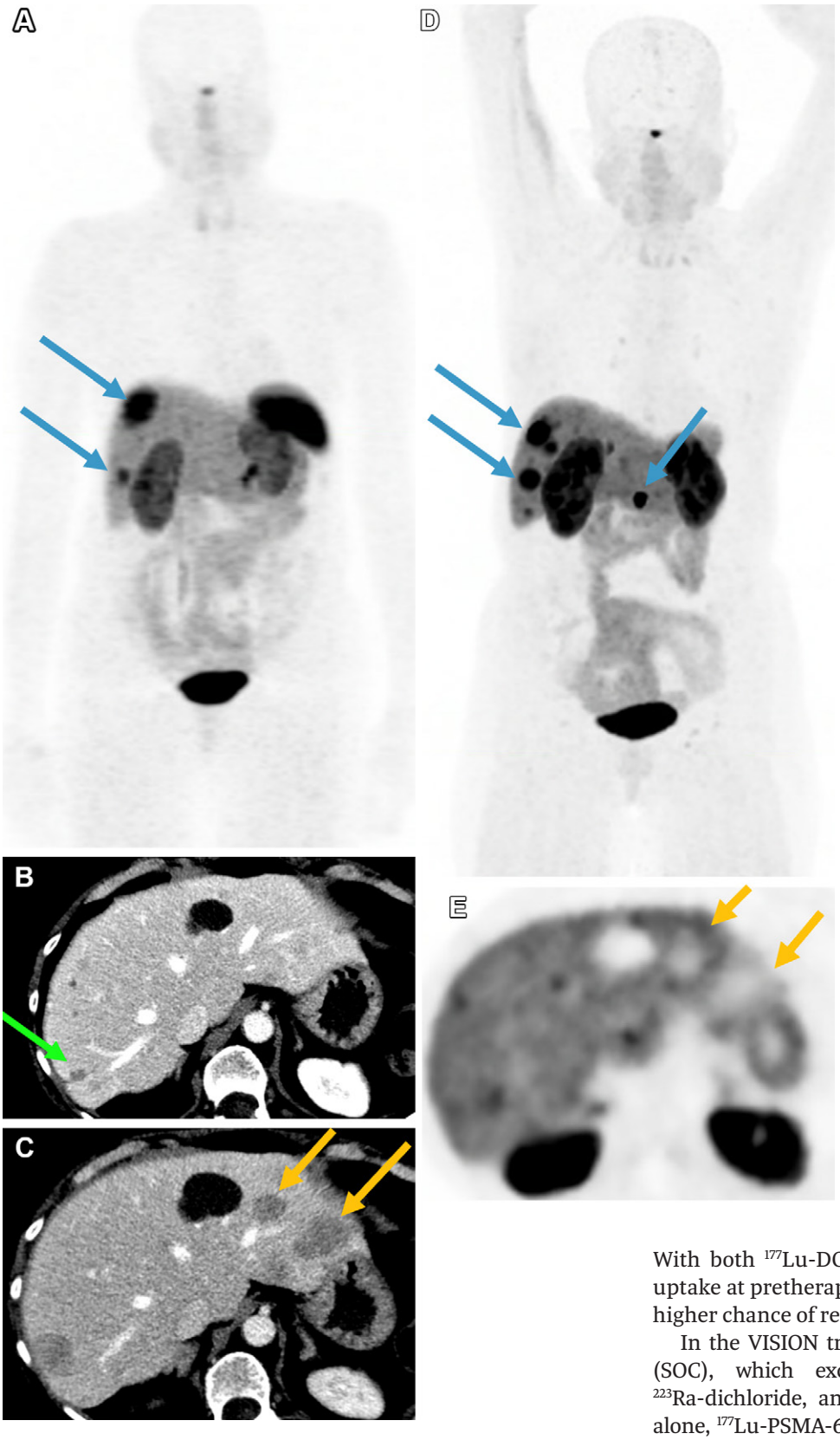

Figure 19. Temporal heterogeneity in a 65-year-old woman with a World Health Organization (WHO) grade 3 well-differentiated pancreatic neuroendocrine tumor. ^{68}Ga-DOTATATE PET/CT was performed for staging. **(A)** Coronal MIP image shows intense uptake in liver metastases (arrows). The patient underwent distal pancreatectomy and splenectomy in addition to liver debulking. **(B)** Postoperative axial CT image with intravenous contrast material shows changes of wedge resection in segment 7 (arrow). **(C)** Axial image from CT with intravenous contrast material performed for follow-up 4 years later shows new liver lesions (arrows). **(D)** Coronal MIP image from ^{68}Ga-DOTATATE PET/CT shows several liver lesions demonstrating DOTATATE uptake (arrows). **(E)** However, axial PET image shows that the new lesions in the left hepatic lobe lack uptake (arrows), consistent with loss of somatostatin receptor expression.

It has been well demonstrated that patients meeting eligibility criteria do not all respond equally to RPT. The level of tumor expression of the RPT target can help predict the response to the therapy. One surrogate metric for this target expression is the level of tumor uptake of the imaging agent. With both ^{177}Lu-DOTATATE and ^{177}Lu-PSMA therapies, high uptake at pretherapy PET has been shown to correlate with a higher chance of response to treatment (31,32,69–71).

In the VISION trial, the control arm was standard of care (SOC), which excluded chemotherapy, immunotherapy, ^{223}Ra-dichloride, and investigational drugs. Relative to SOC alone, ^{177}Lu-PSMA-617 plus SOC significantly prolonged imaging-based progression-free survival (8.7 vs 3.4 months) and overall survival (15.3 vs 11.3 months).

The TheraP trial, a phase III trial that compared ^{177}Lu–PSMA-617 to cabazitaxel in patients with metastatic castration-resistant prostate cancer, used more stringent selection criteria with dual-tracer imaging (PSMA and fluorodeoxyglucose

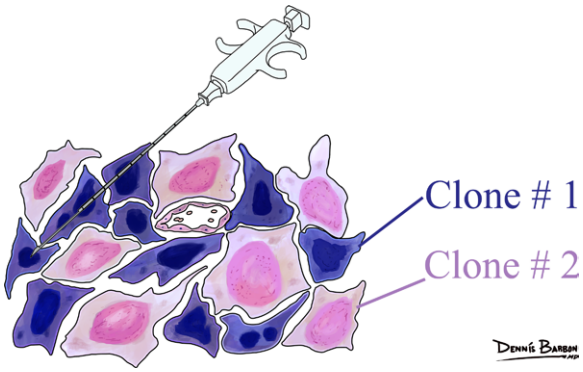

Figure 20. In heterogeneous tumors, there is potential for sampling error. In the example shown, the biopsy would detect clone 1 but undersample clone 2.

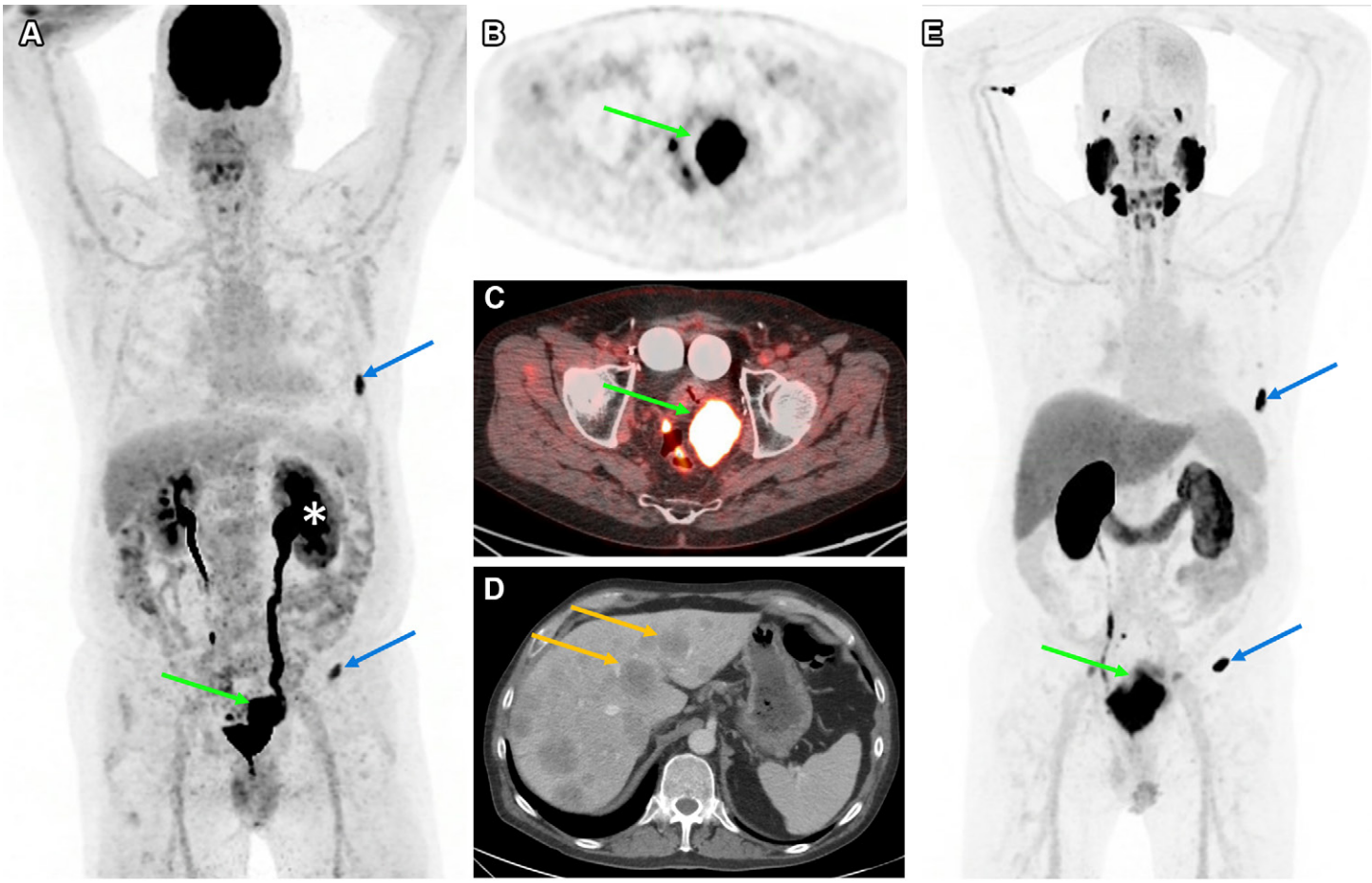

Figure 21. Heterogeneous disease in a 64-year-old man with metastatic prostate cancer (Gleason grade = 4 + 5) who underwent radical prostatectomy 15 years earlier, followed by biochemical recurrence, which was treated with androgen deprivation therapy (ADT) and docetaxel, who now presented with an enlarging pelvic mass. Owing to the uncertain cause of the mass at CT at this point, ^{18}F-FDG PET/CT was performed. **(A–C)** Coronal MIP PET/CT **(A)**, axial PET **(B)**, and axial PET/CT **(C)** ^{18}F-FDG images show a hypermetabolic pelvic mass (maximum standardized uptake value [SUV_{max}] = 17) (green arrow) and two osseous lesions (blue arrows in **A**). Note the left hydronephrosis (∗ in **A**) due to involvement of the left ureter by the pelvic mass. Biopsy of the mass showed metastatic prostate adenocarcinoma, representing local recurrence. This was an uncommon case of a mass producing a low prostate-specific antigen (PSA) level, with PSA level of 0.2 ng/mL at this time. Systemic treatment was restarted. **(D)** Axial image from follow-up CT of the abdomen and pelvis with intravenous contrast material 3 months later shows rapid progression with new liver lesions (arrows). Therefore, PSMA PET/CT with ^{18}F-DCFPyL was performed. **(E, F)** Coronal MIP PET/CT **(E)** and axial PET **(F)** ^{18}F-DCFPyL images show low PSMA expression in the liver metastases (arrows in **F**), which have uptake less than that of background liver (score = 1). PSMA expression is present in the pelvic mass (green arrow in **E**), which has intermediate PSMA expression (score = 2), and in the osseous metastases (blue arrows in **E**), which have high PSMA expression (score = 3). Findings were consistent with heterogeneous disease. Owing to the low PSMA expression in the liver metastases, the patient was not eligible for therapy with ^{177}Lu-PSMA.

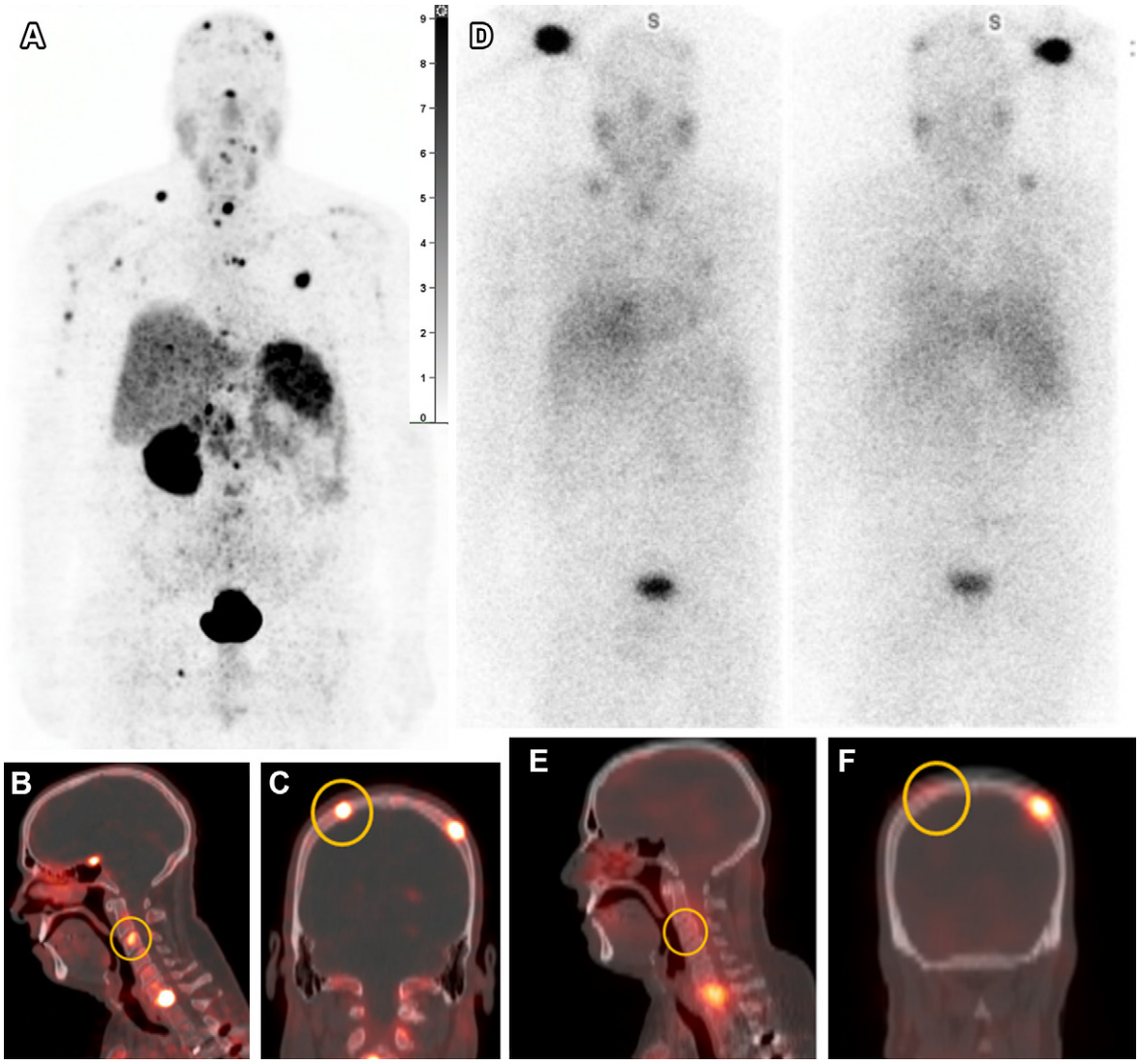

Figure 22. Progressing metastatic paraganglioma in a 55-year-old man who was referred for RPT. To decide on the best treatment option, both DOTATATE and MIBG scans were obtained. Coronal MIP **(A)**, sagittal **(B)**, and coronal **(C)** ^{64}Cu-DOTATATE PET/CT images and anterior (left) and posterior (right) projection planar images from ^{131}I-MIBG scanning **(D)** show uptake in osseous metastases with both tracers. The more intense uptake at DOTATATE PET is expected because of the difference in modality (PET has higher sensitivity than SPECT); to evaluate for discordant lesion uptake with both tracers, SPECT/CT was performed with the MIBG scan. Sagittal **(B)** and coronal **(C)** fused ^{64}Cu-DOTATATE PET/CT images show somatostatin receptor expression within a few osseous lesions (yellow circles) that lack MIBG uptake on the sagittal **(E)** and coronal **(F)** SPECT/CT images. On the basis of these results, the patient was selected for ^{177}Lu-DOTATATE therapy.

[FDG]); eligibility was defined as PSMA-positive disease with maximum standardized uptake value (SUV_{max}) greater than or equal to 20 at a site of disease and greater than 10 at all other measurable sites of disease and no discordant FDG-positive/PSMA-negative sites. This study showed superiority of RPT to cabazitaxel, with greater prostate-specific antigen (PSA) level decline of 50% or more (66% vs 37%) and objective response at imaging (49% vs 24%) (72). As such, the degree of PSMA and DOTATATE uptake at pretherapy imaging is often considered a predictive biomarker.

FDG PET is complementary to DOTATATE and PSMA PET and can be useful for detecting tumor heterogeneity, particularly for identifying hypermetabolic disease that may lack expression of the molecular target. FDG is a prognostic biomarker; hypermetabolic disease is typically more aggressive and is associated with a worse outcome (71,73). It has been shown that despite being eligible for treatment, patients with neuroendocrine tumors or prostate cancer treated with RPT who demonstrate hypermetabolic disease at FDG PET have significantly worse overall survival relative to patients who do not, with emerging evidence supporting the prognostic role of dual-tracer imaging with DOTATATE/FDG PET and PSMA/FDG PET for neuroendocrine tumors and prostate cancer, respectively (61,62,74,75).

This growing body of literature highlights the important role of molecular imaging in guiding disease management. RPTs have already been shown to improve the survival and quality of life of patients who have demonstrated progression

with other treatment modalities. With appropriate patient selection and consideration of imaging biomarkers, there is great interest in introducing RPTs earlier in the treatment paradigm, with the hope of further improving patient outcomes.

Conclusion

The exciting growth of the field of radiotheranostics is improving the survival and quality of life for countless patients. This growth has in turn fueled investigation and development of new agents as well as expansion of indications for approved therapies. While RPTs are a major step toward precision medicine, this approach can be elevated further by working on better understanding the patient-specific factors that contribute to organ toxicity and the tumor factors that play a role in determining treatment response. Tailoring of treatment to individual patients presents the potential of bringing us closer to a paradigm of personalized disease management.

Author affiliations.—From the Medical Scientist Training Program, Feinberg School of Medicine, Northwestern University, Chicago, Ill (A.J.H.S.); and Department of Diagnostic Radiology, Oregon Health and Science University, 3181 SW Sam Jackson Park Rd, L340, Portland, OR 97239-3098 (C.M., A.M., C.W., D.B., S.O., N.M.). Presented as an education exhibit at the 2022 RSNA Annual Meeting. Received April 18, 2023; revision requested June 7 and received June 30; accepted July 10. **Address correspondence to** N.M. (email: *mallak@ohsu.edu*).

Disclosures of conflicts of interest.—**D.B.** Royalties from Elsevier. **N.M.** Grant funding from Blue Earth Diagnostics and Progenics Pharmaceuticals, served on Lantheus advisory board, travel support from the North American Neuroendocrine Tumor Society and Telix Pharmaceuticals. All other authors, the editor, and the reviewers have disclosed no relevant relationships.

References

1. Hertz S, Roberts A, Evans RD. Radioactive Iodine as an Indicator in the Study of Thyroid Physiology. Proceedings of the Society for Experimental Biology and Medicine 1938;38(4):510–513.
2. Pluvicto (lutetium Lu 177 vipivotide tetraxetan) injection. Package insert. Novartis Pharmaceuticals, 2022.
3. Lutathera (lutetium Lu 177 dotatate) injection. Package insert. Novartis Pharmaceuticals, 2018.
4. Azedra (iobenguane I 131) injection. Progenics Pharmaceuticals, 2018.
5. Funkhouser J. Reinventing pharma: the theranostic revolution. Curr Drug Discov 2002;2:17–19.
6. Bartlett RM, Bolch WE, Brill AB, et al. MIRD Primer 2022. Reston, Va: Society of Nuclear Medicine, 2021.
7. Kozempel J, Mokhodoeva O, Vlk M. Progress in Targeted Alpha-Particle Therapy: What We Learned about Recoils Release from In Vivo Generators. Molecules 2018;23(3):581.
8. Sgouros G, Bodei L, McDevitt MR, Nedrow JR. Radiopharmaceutical therapy in cancer: clinical advances and challenges. Nat Rev Drug Discov 2020;19(9):589–608. [Published correction appears in Nat Rev Drug Discov 2020;19(11):819.]
9. Ku A, Facca VJ, Cai Z, Reilly RM. Auger electrons for cancer therapy: a review. EJNMMI Radiopharm Chem 2019;4(1):27.
10. Mulford DA, Scheinberg DA, Jurcic JG. The promise of targeted α-particle therapy. J Nucl Med 2005;46(suppl 1):199S–204S.
11. Emami B, Lyman J, Brown A, et al. Tolerance of normal tissue to therapeutic irradiation. Int J Radiat Oncol Biol Phys 1991;21(1):109–122.
12. Wahl RL, Sgouros G, Iravani A, et al. Normal-Tissue Tolerance to Radiopharmaceutical Therapies, the Knowns and the Unknowns. J Nucl Med 2021;62(suppl 3):23S–35S.
13. Sartor O, de Bono J, Chi KN, et al; VISION Investigators. Lutetium-177-PSMA-617 for Metastatic Castration-resistant Prostate Cancer. N Engl J Med 2021;385(12):1091–1103.
14. Afshar-Oromieh A, Hetzheim H, Kratochwil C, et al. The Theranostic PSMA Ligand PSMA-617 in the Diagnosis of Prostate Cancer by PET/CT: Biodistribution in Humans, Radiation Dosimetry, and First Evaluation of Tumor Lesions. J Nucl Med 2015;56(11):1697–1705.
15. Ehrhardt JD Jr, Güleç S. A Review of the History of Radioactive Iodine Theranostics: the Origin of Nuclear Ontology [in Turkish]. Mol Imaging Radionucl Ther 2020;29(3):88–97.
16. Pathmanandavel S, Crumbaker M, Ho B, et al. Evaluation of 177Lu-PSMA-617 SPECT/CT Quantitation as a Response Biomarker within a Prospective 177Lu-PSMA-617 and NOX66 Combination Trial (LuPIN). J Nucl Med 2023;64(2):221–226.
17. John N, Pathmanandavel S, Crumbaker M, et al. 177Lu-PSMA SPECT Quantitation at 6 Weeks (Dose 2) Predicts Short Progression-free Survival for Patients Undergoing 177Lu-PSMA-I&T Therapy. J Nucl Med 2023;64(3):410–415.
18. Aalbersberg EA, de Vries-Huizing DMV, Tesselaar MET, Stokkel MPM, Versleijen MWJ. Post-PRRT scans: which scans to make and what to look for. Cancer Imaging 2022;22(1):29.
19. Price JM, Prabhakaran A, West CML. Predicting tumour radiosensitivity to deliver precision radiotherapy. Nat Rev Clin Oncol 2023;20(2):83–98.
20. Colton M, Cheadle EJ, Honeychurch J, Illidge TM. Reprogramming the tumour microenvironment by radiotherapy: implications for radiotherapy and immunotherapy combinations. Radiat Oncol 2020;15(1):254.
21. The 2007 Recommendations of the International Commission on Radiological Protection. ICRP publication 103. Ann ICRP 2007;37(2-4):1–332.
22. Bodei L, Modlin IM, Luster M, et al. Myeloid neoplasms after chemotherapy and PRRT: myth and reality. Endocr Relat Cancer 2016;23(8):C1–C7.
23. Bodei L, Kidd M, Paganelli G, et al. Long-term tolerability of PRRT in 807 patients with neuroendocrine tumours: the value and limitations of clinical factors. Eur J Nucl Med Mol Imaging 2015;42(1):5–19.
24. Brieau B, Hentic O, Lebtahi R, et al. High risk of myelodysplastic syndrome and acute myeloid leukemia after 177Lu-octreotate PRRT in NET patients heavily pretreated with alkylating chemotherapy. Endocr Relat Cancer 2016;23(5):L17–L23.
25. Feuerecker B, Tauber R, Knorr K, et al. Activity and Adverse Events of Actinium-225-PSMA-617 in Advanced Metastatic Castration-resistant Prostate Cancer after Failure of Lutetium-177-PSMA. Eur Urol 2021;79(3):343–350.
26. Ballal S, Yadav MP, Bal C, Sahoo RK, Tripathi M. Broadening horizons with 225Ac-DOTATATE targeted alpha therapy for gastroenteropancreatic neuroendocrine tumour patients stable or refractory to 177Lu-DOTATATE PRRT: first clinical experience on the efficacy and safety. Eur J Nucl Med Mol Imaging 2020;47(4):934–946.
27. Haberkorn U, Giesel F, Morgenstern A, Kratochwil C. The Future of Radioligand Therapy: α, β, or Both? J Nucl Med 2017;58(7):1017–1018.
28. Hope TA, Antonarakis ES, Bodei L, et al. SNMMI Consensus Statement on Patient Selection and Appropriate Use of 177Lu-PSMA-617 Radionuclide Therapy. J Nucl Med 2023. 10.2967/jnumed.123.265952. Published online June 8, 2023.
29. Vallathol DH, Digumarti RAN. An Update on Toxicity of Theraputic Radionuclides. Med Res Arch 2021;9(4). https://doi.org/10.18103/mra.v9i4.2388.
30. Schreuder N, de Romijn I, Jager PL, Kosterink JGW, van Puijenbroek EP. Safe use of radiopharmaceuticals in patients with chronic kidney disease: a systematic review. EJNMMI Radiopharm Chem 2021;6(1):27.
31. Vlachostergios PJ, Niaz MJ, Skafida M, et al. Imaging expression of prostate-specific membrane antigen and response to PSMA-targeted β-emitting radionuclide therapies in metastatic castration-resistant prostate cancer. Prostate 2021;81(5):279–285.
32. Sharma R, Wang WM, Yusuf S, et al. 68Ga-DOTATATE PET/CT parameters predict response to peptide receptor radionuclide therapy in neuroendocrine tumours. Radiother Oncol 2019;141:108–115.
33. Seifert R, Emmett L, Rowe SP, et al. Second Version of the Prostate Cancer Molecular Imaging Standardized Evaluation Framework Including Response Evaluation for Clinical Trials (PROMISE V2). Eur Urol 2023;83(5):405–412.
34. Chiesa C, Sjogreen Gleisner K, Flux G, et al. The conflict between treatment optimization and registration of radiopharmaceuticals with fixed activity posology in oncological nuclear medicine therapy. Eur J Nucl Med Mol Imaging 2017;44(11):1783–1786.
35. Flux GD, Sjogreen Gleisner K, Chiesa C, et al. From fixed activities to personalized treatments in radionuclide therapy: lost in translation? Eur J Nucl Med Mol Imaging 2018;45(1):152–154.
36. Lassmann M, Eberlein U. The Relevance of Dosimetry in Precision Medicine. J Nucl Med 2018;59(10):1494–1499.
37. Strigari L, Konijnenberg M, Chiesa C, et al. The evidence base for the use of internal dosimetry in the clinical practice of molecular radiotherapy. Eur J Nucl Med Mol Imaging 2014;41(10):1976–1988.
38. Kwekkeboom DJ, Bakker WH, Kam BL, et al. Treatment of patients with gastro-entero-pancreatic (GEP) tumours with the novel radiolabelled somatostatin analogue [177Lu-DOTA(0),Tyr3]octreotate. Eur J Nucl Med Mol Imaging 2003;30(3):417–422.

39. Benua RS, Cicale NR, Sonenberg M, Rawson RW. The relation of radioiodine dosimetry to results and complications in the treatment of metastatic thyroid cancer. Am J Roentgenol Radium Ther Nucl Med 1962;87:171–182.
40. Ljungberg M, Celler A, Konijnenberg MW, et al; SNMMI MIRD Committee; EANM Dosimetry Committee. MIRD Pamphlet no. 26: Joint EANM/MIRD Guidelines for Quantitative 177Lu SPECT Applied for Dosimetry of Radiopharmaceutical Therapy. J Nucl Med 2016;57(1):151–162.
41. Siegel JA, Thomas SR, Stubbs JB, et al. MIRD pamphlet no. 16: techniques for quantitative radiopharmaceutical biodistribution data acquisition and analysis for use in human radiation dose estimates. J Nucl Med 1999;40(2):37S–61S.
42. Dewaraja YK, Frey EC, Sgouros G, et al. MIRD pamphlet no. 23: quantitative SPECT for patient-specific 3-dimensional dosimetry in internal radionuclide therapy. J Nucl Med 2012;53(8):1310–1325.
43. Sjögreen Gleisner K, Chouin N, Gabina PM, et al. EANM dosimetry committee recommendations for dosimetry of 177Lu-labelled somatostatin-receptor- and PSMA-targeting ligands. Eur J Nucl Med Mol Imaging 2022;49(6):1778–1809.
44. Hou X, Brosch J, Uribe C, et al. Feasibility of Single-Time-Point Dosimetry for Radiopharmaceutical Therapies. J Nucl Med 2021;62(7):1006–1011.
45. Jackson PA, Hofman MS, Hicks RJ, Scalzo M, Violet J. Radiation Dosimetry in 177Lu-PSMA-617 Therapy Using a Single Posttreatment SPECT/CT Scan: a Novel Methodology to Generate Time- and Tissue-specific Dose Factors. J Nucl Med 2020;61(7):1030–1036.
46. Willowson KP, Eslick E, Ryu H, Poon A, Bernard EJ, Bailey DL. Feasibility and accuracy of single time point imaging for renal dosimetry following 177Lu-DOTATATE ('Lutate') therapy. EJNMMI Phys 2018;5(1):33.
47. Release of individuals containing unsealed byproduct material or implants containing byproduct material. U.S. Nuclear Regulatory Commission. https://www.nrc.gov/reading-rm/doc-collections/cfr/part035/part035-0075.html. Updated August 29, 2017. Accessed April 10, 2023.
48. Xofigo (radium Ra 223 dichloride) Injection. Package insert. Bayer HealthCare Pharmaceuticals, 2013.
49. Shaffer V. Release of patients administered radioactive material. U.S. Nuclear Regulatory Commission. https://www.nrc.gov/reading-rm/doc-collections/cfr/part035/part035-0075.html. Published April 2020. Accessed April 10, 2023.
50. Dentro SC, Leshchiner I, Haase K, et al; PCAWG Evolution and Heterogeneity Working Group and the PCAWG Consortium. Characterizing genetic intra-tumor heterogeneity across 2,658 human cancer genomes. Cell 2021;184(8):2239–2254.e39.
51. Goyal Y, Dardani IP, Busch GT, et al. Pre-determined diversity in resistant fates emerges from homogenous cells after anti-cancer drug treatment. bioRxiv 2021:2021.12.08.471833. DOI: https://doi.org/10.1101/2021.12.08.471833.
52. Botling J, Lamarca A, Bajic D, et al. High-Grade Progression Confers Poor Survival in Pancreatic Neuroendocrine Tumors. Neuroendocrinology 2020;110(11-12):891–898.
53. Marusyk A, Janiszewska M, Polyak K. Intratumor Heterogeneity: the Rosetta Stone of Therapy Resistance. Cancer Cell 2020;37(4):471–484.
54. Eisenhauer EA, Therasse P, Bogaerts J, et al. New Response Evaluation Criteria in Solid Tumours: revised RECIST guideline (version 1.1). Eur J Cancer 2009;45(2):228–247.
55. O'Connor JPB, Rose CJ, Waterton JC, Carano RAD, Parker GJM, Jackson A. Imaging intratumor heterogeneity: role in therapy response, resistance, and clinical outcome. Clin Cancer Res 2015;21(2):249–257.
56. Keek SA, Leijenaar RT, Jochems A, Woodruff HC. A review on radiomics and the future of theranostics for patient selection in precision medicine. Br J Radiol 2018;91(1091):20170926.
57. Werner RA, Ilhan H, Lehner S, et al. Pre-therapy Somatostatin Receptor-based Heterogeneity Predicts Overall Survival in Pancreatic Neuroendocrine Tumor Patients Undergoing Peptide Receptor Radionuclide Therapy. Mol Imaging Biol 2019;21(3):582–590. [Published correction to Mol Imaging Biol 2018;20(6):1068.]
58. Wetz C, Genseke P, Apostolova I, et al. The association of intra-therapeutic heterogeneity of somatostatin receptor expression with morphological treatment response in patients undergoing PRRT with [177Lu]-DOTATATE. PLoS One 2019;14(5):e0216781.
59. Khurshid Z, Ahmadzadehfar H, Gaertner FC, et al. Role of textural heterogeneity parameters in patient selection for 177Lu-PSMA therapy via response prediction. Oncotarget 2018;9(70):33312–33321.
60. Fourquet A, Rosenberg A, Mena E, et al. A Comparison of 18F-DCFPyL, 18F-NaF, and 18F-FDG PET/CT in a Prospective Cohort of Men with Metastatic Prostate Cancer. J Nucl Med 2022;63(5):735–741.
61. Chan DL, Pavlakis N, Schembri GP, et al. Dual Somatostatin Receptor/FDG PET/CT Imaging in Metastatic Neuroendocrine Tumours: Proposal for a Novel Grading Scheme with Prognostic Significance. Theranostics 2017;7(5):1149–1158.
62. Chan DL, Hayes AR, Karfis I, et al. Dual [68Ga]DOTATATE and [18F]FDG PET/CT in patients with metastatic gastroenteropancreatic neuroendocrine neoplasms: a multicentre validation of the NETPET score. Br J Cancer 2023;128(4):549–555.
63. Hope TA, Abbott A, Colucci K, et al. NANETS/SNMMI Procedure Standard for Somatostatin Receptor-based Peptide Receptor Radionuclide Therapy with 177Lu-DOTATATE. J Nucl Med 2019;60(7):937–943.
64. Graf J, Pape UF, Jann H, et al. Prognostic Significance of Somatostatin Receptor Heterogeneity in Progressive Neuroendocrine Tumor Treated with Lu-177 DOTATOC or Lu-177 DOTATATE. Eur J Nucl Med Mol Imaging 2020;47(4):881–894.
65. Strosberg J, El-Haddad G, Wolin E, et al; NETTER-1 Trial Investigators. Phase 3 Trial of 177Lu-Dotatate for Midgut Neuroendocrine Tumors. N Engl J Med 2017;376(2):125–135.
66. Pryma DA, Chin BB, Noto RB, et al. Efficacy and Safety of High-Specific-Activity 131I-MIBG Therapy in Patients with Advanced Pheochromocytoma or Paraganglioma. J Nucl Med 2019;60(5):623–630.
67. Shah MH, Goldner WS, Halfdanarson TR, et al. NCCN Guidelines Insights: Neuroendocrine and Adrenal Tumors, Version 2.2018. J Natl Compr Canc Netw 2018;16(6):693–702.
68. Carrasquillo JA, Chen CC, Jha A, Pacak K, Pryma DA, Lin FI. Systemic Radiopharmaceutical Therapy of Pheochromocytoma and Paraganglioma. J Nucl Med 2021;62(9):1192–1199.
69. Hotta M, Gafita A, Murthy V, et al. PSMA PET Tumor-to-Salivary Gland Ratio to Predict Response to [177Lu]PSMA Radioligand Therapy: an International Multicenter Retrospective Study. J Nucl Med 2023;64(7):1024–1029.
70. Öksüz MÖ, Winter L, Pfannenberg C, et al. Peptide receptor radionuclide therapy of neuroendocrine tumors with (90)Y-DOTATOC: is treatment response predictable by pre-therapeutic uptake of (68)Ga-DOTATOC? Diagn Interv Imaging 2014;95(3):289–300.
71. Buteau JP, Martin AJ, Emmett L, et al; TheraP Trial Investigators and the Australian and New Zealand Urogenital and Prostate Cancer Trials Group. PSMA and FDG-PET as predictive and prognostic biomarkers in patients given [177Lu]Lu-PSMA-617 versus cabazitaxel for metastatic castration-resistant prostate cancer (TheraP): a biomarker analysis from a randomised, open-label, phase 2 trial. Lancet Oncol 2022;23(11):1389–1397.
72. Hofman MS, Emmett L, Sandhu S, et al; TheraP Trial Investigators and the Australian and New Zealand Urogenital and Prostate Cancer Trials Group. [177Lu]Lu-PSMA-617 versus cabazitaxel in patients with metastatic castration-resistant prostate cancer (TheraP): a randomised, open-label, phase 2 trial. Lancet 2021;397(10276):797–804.
73. Binderup T, Knigge U, Loft A, Federspiel B, Kjaer A. 18F-fluorodeoxyglucose positron emission tomography predicts survival of patients with neuroendocrine tumors. Clin Cancer Res 2010;16(3):978–985.
74. Binderup T, Knigge U, Johnbeck CB, et al. 18F-FDG PET is Superior to WHO Grading as a Prognostic Tool in Neuroendocrine Neoplasms and Useful in Guiding PRRT: a Prospective 10-year Follow-up Study. J Nucl Med 2021;62(6):808–815.
75. Michalski K, Ruf J, Goetz C, et al. Prognostic implications of dual tracer PET/CT: PSMA ligand and [18F]FDG PET/CT in patients undergoing [177Lu]PSMA radioligand therapy. Eur J Nucl Med Mol Imaging 2021;48(6):2024–2030.